Applications of Supported Lipid Bilayers and
Nanolipoprotein Particles

By

AMANDA T. DANG
DISSERTATION

Submitted in partial satisfaction of the requirements for the degree of

DOCTOR OF PHILOSOPHY

in

Materials Science and Engineering

in the

OFFICE OF GRADUATE STUDIES

of the

UNIVERSITY OF CALIFORNIA

DAVIS

Approved:

Prof. Tonya Kuhl, Chair

Prof. Marjorie Longo

Dr. Matthew Coleman

Committee in Charge
2019

Dedication

For my loving parents, Kenneth C. Dang, Nha Diep, Anh Dao Phan, and my dear sister, Nina.

Amanda Tuyet-Yi Dang
September 2019
Materials Science and Engineering

Applications of Supported Lipid Bilayers and Nanolipoprotein Particles

Abstract

Since dysregulation of membrane proteins (MPs) is commonly implicated in disease onset and progression, there is compelling motivation to attain knowledge of MP structure and behavior to inform targeted drug design. MPs are typically difficult to characterize because they require the unique environment of a lipid bilayer to assume their native functional conformations. One way to address this obstacle is by utilizing biomimetic model systems which recapitulate the fundamental properties of naturally occurring membranes under well-defined conditions. The works compiled in this dissertation focus on the fabrication, characterization, and application of two types of experimental platforms - The supported lipid bilayer (SLB) and the nanolipoprotein particle (NLP). The SLB is a lipid bilayer that has been reconstituted on a planar solid support. A nanolipoprotein particle (NLP) is a lipid bilayer disc stabilized by two amphipathic "scaffold" apolipoproteins. Importantly, the NLP is capable of solubilizing functional MPs by forming stable MP-NLP complexes using straightforward preparation methods. SLBs serve as reliable platforms for studying a variety of membrane phenomena but have traditionally been challenging targets for incorporation of MPs. We explore NLP-mediated delivery as a potential solution to this issue. Experimental results revealed that transfer of lipids and proteins from NLPs to SLBs occurs spontaneously under ambient conditions. Optimal conditions for enhancing delivery are also described.

Table of Contents

Chapter 1: Introduction 1

References 2

Chapter 2: Adaptive Cytoskeleton Mimetic for Biomembrane Applications 4

Introduction 5

Materials 7

Methods 8
Preparation of PAA-Coated Surfaces 8
Deposition of Lipid Bilayers 9
Fluorescence Recovery After Photobleaching (FRAP) 10
Neutron Reflectivity 11

Results and Discussion 12
Properties of Poly(Acrylic Acid) (PAA) Cushions 12
PAA Films in Air 13
PAA-Cushioned Membranes 14
Hybrid LB/Vesicle Fusion of PAA-Cushioned Membranes 18
Membrane Diffusion 18
Influence of Initial PAA Thickness and pH on Diffusion 20
Diffusion of PAA-Cushioned Membranes under Physiological Conditions 21
Comparison to Reported Diffusion Coefficient Values 22

Conclusion 22

Acknowledgements 24

References 24

Chapter 3: Lipid and Protein Transfer between Nanolipoprotein Particles and Supported Lipid Bilayers 28

Introduction 29

Materials and Methods 31
General Materials and Methods 31
PAA Cushion Preparation 33
SLB Sample Preparation 33
Vesicle Sample Preparation 34
NLP Assembly from Lyophilized Apolipoprotein 34
NLP Assembly using Cell-Free Expression 35
NLP Purification and Verification 35
NLP Incubation with SLBs 36
Fluorescence Microscopy 36
Atomic Force Microscopy 37

Results 37
Impact of SLB Composition on Lipid Exchange 37
AFM of SLBs Incubated with NLPs 40
Lipid Transfer between NLPs and PAA-Cushioned SLBs 43
Mechanisms of Transfer 46

Conclusions 46

Associated Content 48

Author Information 48
Funding Sources 48
Acknowledgement *49*
References *49*
Supporting Information *53*
Chapter 4: Mind the line tension – A new criteria for nanodomains in biological membranes 60
References *63*
Chapter 5: Theoretical Interaction Energies between a Silica Surface and a Phospholipid Bilayer 64
Project Background *64*
Electrostatic Energy Contribution *64*
Van der Waals Energy Contribution *66*
Zeta Potential Measurement *66*
Determining Surface Charge Density from Zeta Potential *67*
References *67*
Chapter 6: Experimental Considerations 68
Fabrication of PAA-cushioned Supported Lipid Bilayers *68*
AFM of Supported Lipid Bilayers and Nanolipoprotein Particles *68*
Fluorescence Microscopy of SLBs *69*
UV-Ozone Patterning of Supported Lipid Bilayers *69*
Fabrication and Characterization of Nanolipoprotein Particles *70*
Incubation of SLBs with NLPs *71*

Chapter 1: Introduction

The cell membrane is a compositionally complex phospholipid bilayer that hosts an important class of proteins known as, membrane proteins (MPs) or integral membrane proteins (IMP).[1] MPs play pronounced roles in critical cell processes including, adhesion, signal transduction, and carrier-mediated transport.[2] Accordingly, MP-related dysregulation can lead to disease onset and progression.[3-4] Approximately 60% of currently marketed drugs achieve therapeutic effect by targeting MPs[5] even though MPs make up less than 1% of solved high-resolution structures.[6] In addition to improved understanding of molecular mechanisms which underlie important biological processes, comprehensive characterization of these functional biomolecules could accelerate progress in structure-based drug design[7] and lead to superior homology models for screening of receptor binding compounds.[8]

Over the past two decades, gradual improvements in protein crystallization methodologies, Cryo-electron microscopy (Cryo-EM), nuclear magnetic resonance (NMR) spectroscopy, and X-ray scattering techniques have paved the way for a growing cache of solved MP structures.[8-13] Yet, MPs remain extremely difficult to produce, solubilize, and manipulate. Because MPs typically contain hydrophobic domains which anchor preferentially into one or both sides of the phospholipid bilayer, they are prone to denaturation or misfolding when removed from native membrane environments. To present MPs with high fidelity in a non-native environment, it is necessary to use a biomimetic system which presents a compartmentalized structure akin to that of a biological membrane.[14]

The works compiled in this dissertation focus on the development of two types of model membrane systems – The supported lipid bilayer (SLB) and the nanolipoprotein particle (NLP) a.k.a. nanodisc – Into broadly applicable tools for membrane protein characterization. The planar SLB, described in detail in Chapter 2, lends itself to surface-sensitive characterization methods which could be used to probe MP structure. However, application of SLBs for investigation of MPs has traditionally been hindered

by challenges associated with integrating MPs into the SLB. This project aimed to address this issue by way of NLP-mediated transport of functional MPs into SLBs. Described in detail in Chapter 3, the NLP was found to be a viable delivery vehicle for introducing both lipids and MPs into SLBs under physiological saline conditions. Subsequent efforts to optimize delivery revealed that transfer could be enhanced by increasing the concentration of defects or incorporating NLP-binding molecules in the target SLB. Additional content on fundamental properties of SLBs and experimental considerations are provided in Chapters 4-5 and Chapter 6, respectively.

References

1. Bruce Alberts, A. J., Julian Lewis, Martin Raff, Keith Roberts, Peter Walter, Protein Function. In *Molecular Biology of the Cell*, 4th ed.; Garland Science: New York, 2002.
2. Lodish H, B. A., Zipursky SL, et al., Section 3.4, Membrane Proteins. In *Molecular Cell Biology*, 4th ed.; W. H. Freeman: New York, 2000.
3. Roskoski Jr, R., The ErbB/HER family of protein-tyrosine kinases and cancer. *Pharmacological Research* **2014,** *79*, 34-74.
4. Roskoski, R., ErbB/HER protein-tyrosine kinases: Structures and small molecule inhibitors. *Pharmacological Research* **2014,** *87*, 42-59.
5. Früh, V.; Zhou, Y.; Chen, D.; Loch, C.; Eiso, A. B.; Grinkova, Y. N.; Verheij, H.; Sligar, S. G.; Bushweller, J. H.; Siegal, G., Application of Fragment Based Drug Discovery to Membrane Proteins: Biophysical Identification of Ligands of the Integral Membrane Enzyme DsbB. *Chemistry & biology* **2010,** *17* (8), 881-891.
6. White, S. Membrane Proteins of Known 3D Structure. http://blanco.biomol.uci.edu/mpstruc/ (accessed 21 January).
7. Grey, J.; Thompson, D., Challenges and Opportunities for New Protein Crystallization Strategies in Structure-Based Drug Design. *Expert opinion on drug discovery* **2010,** *5* (11), 1039-1045.
8. Stockert, J. A.; Devi, L. A., Advancements in therapeutically targeting orphan GPCRs. *Frontiers in Pharmacology* **2015,** *6*, 100.
9. Garrett, T. P.; McKern, N. M.; Lou, M.; Elleman, T. C.; Adams, T. E.; Lovrecz, G. O.; Zhu, H. J.; Walker, F.; Frenkel, M. J.; Hoyne, P. A.; Jorissen, R. N.; Nice, E. C.; Burgess, A. W.; Ward, C. W., Crystal structure of a truncated epidermal growth factor receptor extracellular domain bound to transforming growth factor alpha. *Cell* **2002,** *110* (6), 763-73.
10. Garrett, T. P. J.; McKern, N. M.; Lou, M. Z.; Elleman, T. C.; Adams, T. E.; Lovrecz, G. O.; Kofler, M.; Jorissen, R. N.; Nice, E. C.; Burgess, A. W.; Ward, C. W., The crystal structure of a truncated ErbB2 ectodomain reveals an active conformation, poised to interact with other ErbB receptors. *Mol. Cell* **2003,** *11* (2), 495-505.
11. Ogiso, H.; Ishitani, R.; Nureki, O.; Fukai, S.; Yamanaka, M.; Kim, J.-H.; Saito, K.; Sakamoto, A.; Inoue, M.; Shirouzu, M.; Yokoyama, S., Crystal Structure of the Complex of Human Epidermal Growth

Factor and Receptor Extracellular Domains. *Cell* **2002,** *110* (6), 775-787.

12. Franklin, M. C.; Carey, K. D.; Vajdos, F. F.; Leahy, D. J.; de Vos, A. M.; Sliwkowski, M. X., Insights into ErbB signaling from the structure of the ErbB2-pertuzumab complex. *Cancer Cell* **2004,** *5* (4), 317-328.
13. Stamos, J.; Sliwkowski, M. X.; Eigenbrot, C., Structure of the Epidermal Growth Factor Receptor Kinase Domain Alone and in Complex with a 4-Anilinoquinazoline Inhibitor. *Journal of Biological Chemistry* **2002,** *277* (48), 46265-46272.
14. Raunser, S.; Walz, T., Electron crystallography as a technique to study the structure on membrane proteins in a lipidic environment. *Annual review of biophysics* **2009,** 38, 89-105.

Chapter 2: Adaptive Cytoskeleton Mimetic for Biomembrane Applications

Caroline Y. Kim[1†], Amanda T. Dang[2†], Simon Castorph[1], Rita J. El-Khouri[3¥], Erik Watkins[4‡], Tonya L. Kuhl[1]

[1]Department of Chemical Engineering, University of California, Davis CA
[2]Department of Materials Science and Engineering, University of California, Davis CA
[3]Department of Chemistry, University of California, Davis CA
[4]Biophysics Graduate Group, University of California, Davis CA
[†]Both authors contributed equally
[¥]Current address: Method Products, pbc. San Francisco CA
[‡]MPA-11: Materials Synthesis and Integrated Devices, Los Alamos National Laboratory, Los Alamos NM
*Corresponding author email address: tlkuhl@ucdavis.edu

Keywords: lipid bilayer, monolayer, polymer cushion, scattering, diffraction, DPPC, DMPC, FRAP

Abstract:

The structure and lateral mobility of a polymer-cushioned membrane consisting of a phospholipid bilayer supported on a poly(acrylic acid) (PAA) film was studied by means of neutron reflectivity and fluorescence recovery after photobleaching (FRAP). High quality, high coverage lipid membranes were constructed using either Langmuir-Blodgett (LB)/Langmuir Schaeffer (LS) or hybrid LB/vesicle fusion deposition methods. The pH responsive PAA cushion is easily fabricated from inexpensive, commercially available materials with nominal thickness controlled by spin coating conditions. The pH-sensitive structure of the PAA cushion and coupling to the membrane can be used to control the hydrated thickness of the cushion and membrane diffusivity. It provides a straightforward means to tailor diffusivity and membrane-cushion coupling akin to the cytoskeleton, a biological polymeric network that influences the structure and lateral organization of the cell membrane. At low pH, when the PAA cushion was collapsed, diffusivity was strikingly lower than at high pH when the PAA was swollen. Under physiological conditions, the diffusion rates of lipid membranes on a PAA cushion were indistinguishable from those on bare glass supports. Furthermore, the cushioned membrane structure was stable during cycling through acidic, neutral, and alkaline conditions. Altogether, the results of this work show that PAA provides a robust, structurally tunable interface for biophysical studies of supported membranes, and has potential to serve as a platform for investigation of membrane-embedded proteins and biosensing applications.

Author Contribution Notes:

Neutron reflectometry measurements and analysis were performed by S. Castorph, E. Watkins, and T. L. Kuhl. Fluorescence microscopy and discussion elements were contributed by C. Y. Kim and A. T. Dang.

Introduction

Biological membranes are highly organized, responsive thin films composed of a myriad of lipids and proteins. They are compositionally complex and dynamic in nature, lending themselves to key roles in a multitude of critical cell functions. To investigate specific aspects of biological membranes, biomimetic model platforms such as the supported lipid bilayer (SLB) have emerged as invaluable tools for research. The SLB, which permits refined control over composition and phase in distinction from its biological archetype, has been extensively used to study membrane dynamics, membrane structure, lipid-protein interactions, and integral membrane protein properties.[1-2] Further, the planar geometry of the SLB and conferred stability of the substrate to the supported membrane enables the utilization of a wide variety of surface-sensitive analytical techniques.

Although the SLB is appropriate for many biophysical studies, the close proximity of the solid support to the bilayer can lead to undesirable protein-substrate interactions, alterations to the structure of the supported membrane, and dampened membrane undulations.[3-4] Protein-substrate interactions are the foremost cause for concern because they frequently result in compromised protein function, denaturation, as well as lateral immobilization of proteins within the membrane. One way to overcome these limitations is to introduce a hydrophilic polymer cushion between the membrane and the solid support. By acting as a hydrated spacer, the polymer film effectively prevents membrane-associated biomolecules from interacting with the underlying hard substrate. Undesirable substrate effects such as decreased lateral mobility and limited self-healing of the membrane are therefore ameliorated, and can yield biomembrane properties akin to those of free-standing bilayers.

Polymer-cushioned SLBs can be distinguished based on their manner of preparation. Broadly speaking, there are two basic approaches.[1-2, 5-7] In the first, the polymer layer is deposited onto the substrate and the membrane is subsequently assembled on top of the cushion. [8-14] Cushion materials developed using this methodology include polysaccharides like, dextran,[15] chitosan,[16] agarose,[11] and

cellulose,[17-18] as well as polymers such as, polyethyleneimine,[9-10] polynipam,[19-20] and polyelectrolyte films.[21-24] In the second approach, polymer-functionalized lipids (i.e. lipopolymer tethers) or alkyl side chains capable of inserting into the phospholipid bilayer are incorporated into the membrane itself.[25-28] These additives steady the overall structure and can suspend the membrane over the underlying hard substrate.[7, 14, 25, 29] Hybrid systems consisting of a grafted polymer cushion with embedded polymer-functionalized lipids or polymer-reactive lipids have also been investigated.[30-31]

There are several advantages of polymer-cushioned SLBs compared to those stabilized by conventional inorganic, solid supports (e.g. glass, mica, silicon). First, the hydrophilic polymer cushion enables formation of model membrane platforms that are more structurally evocative of free-standing bilayers. Second, the polymer cushion can screen the membrane and constituent components from interactions with the underlying solid support. Third, the polymer film can be designed to minimize interactions between itself and the lipid bilayer to prevent immobilization or altered functionality of membrane-associated biomolecules. Especially in studies involving transmembrane proteins in SLBs, it is most necessary to select a polymer material that is hydrophilic, flexible, only slightly charged, loosely cross-linked, and less interactive with membrane lipids or proteins.[1, 32] Lastly, the polymer cushion can also be suggestive of a model cytoskeleton or an extracellular matrix.

The cytoskeleton is an important architectural feature that affects lateral compartmentalization and physical structure in the native cellular environment. Comprised of actin filaments, microtubules, and intermediate filaments, the cytoskeleton can orchestrate forces required for cell movement and shape change by polymerizing and depolymerizing in response to external stimuli.[33] Plus, it can affect membrane properties through nonspecific interactions.[34] Polymer-cushioned SLBs are especially useful systems for modeling the symbiotic relationship between these two structures. In addition to inducing an asymmetric environment by coupling to only one side of the bilayer, a polymer cushion be systematically optimized to simulate diverse cytoskeletal conditions. Parameters such as, polymer composition, degree of cross-

linking, and average molecular weight can all be adjusted to induce specific properties in the supported bilayer.[7, 35]

In this work, we report the detailed characterization of a robust, versatile, and pH-sensitive polymer-cushioned SLB which employs a thin spin coated poly(acrylic acid) (PAA) film to elevate the lipid bilayer from the solid support and act as a cytoskeleton analogue. The structure of PAA-cushioned membranes formed by Langmuir-Blodgett (LB)/ Langmuir-Schaeffer (LS) deposition and LB/vesicle fusion was precisely established using neutron reflectivity (NR). Reflectivity results demonstrated that not unlike other documented polyelectrolyte systems,[22, 24, 36-38] PAA-cushioned membranes exhibit pH-dependent swelling properties, with high degree of reversibility when cycling between swollen and collapsed states. Additionally, PAA cushion thickness can be quantitatively tailored for different applications by modifying the concentration of the spin coating solution. To better understand the implications of the state of the PAA cushion on membrane fluidity, the pH dependence of membrane mobility was determined using fluorescence recovery after photo bleaching (FRAP).[39] These experiments revealed that PAA-cushioned SLBs can be manipulated to transition from a relatively fast lipid diffusion rate at physiological and alkaline pH conditions to a relatively slow diffusion rate under acidic conditions. Diffusion coefficient values obtained under physiological and alkaline conditions were equivalent to those obtained from non-cushioned SLBs. In summary, this system offers a reliable and facile means to fabricate supported biological membranes where the influence of the underlying cushion can be tailored for biophysical studies and biosensing applications. Moreover, all of the materials required to produce this platform are inexpensive and readily available.

Materials

1,2-dimyristoleoyl-sn-glycero-3-phosphocholine (DMPC), 1,2-dipalmitoyl-sn-glycerol-3-phosphatidylcholine (DPPC), and tail-deuterated DPPC (dDPPC) were purchased from Avanti Polar lipids (Alabaster, AL). Texas Red® 1,2-dihexadecanoyl-sn-glycero-3-phosphoethanolamine (Texas Red-DHPE) was

purchased from Invitrogen (Carlsbad, CA). Lipids were dissolved in chloroform, HPLC grade, purchased from Fisher Scientific (Fairlawn, NJ) to make solutions at a final concentration of 1 mg/ml. For Neutron Reflectivity (NR) measurements, buffer solutions were primarily made using prefabricated Fluka buffer tablets at pH 4, pH 7, and pH 9. For fluorescence microscopy experiments, citric acid-sodium citrate, sodium-disodium phosphate, and sodium carbonate-bicarbonate buffers were used to create solution conditions at pH 4, pH 7.4, and pH 9.2, respectively. All buffer reagents, poly(acrylic acid) (PAA, MW = 450k, 0.1% cross-linked), and 3-(aminopropyl)triethoxysilane (APTES) were purchased from Sigma-Aldrich (St. Louis, MO) and used without further purification. NR measurements used 3 inch diameter single crystal quartz substrates (c-cut, α-quartz, density 2.64–2.65 gcm^{-3}, Institute of Electronic Materials Technology, Warsaw, Poland). Fluorescence microscopy experiments used 1 inch diameter circular fused quartz substrates (thickness of 0.5 mm, $\lambda/4$ surface roughness) and 18 mm diameter circular microscope cover glass (thickness of 0.2 mm) were purchased from Mark Optics (Santa Ana, CA) and Fisher Scientific (Pittsburgh, PA), respectively.

Methods

Preparation of PAA-Coated Surfaces

Glass and quartz substrates were cleaned according to the following procedure to remove organic residues. Substrates were sonicated for 30 minutes in a strongly basic detergent (Hellmanex, Sigma Aldrich), rinsed in MilliQ water, sonicated for 10 minutes in acetone, then isopropanol, and rinsed again with MilliQ water. Finally, substrates were dried with a stream of nitrogen gas (N_2). The surfaces of clean substrates were hydroxylated by exposure for 20-30 minutes in a UV-Ozone chamber (Jelight Company Inc., Irvine, CA). A UV pen light can also be used for this purpose with typical exposure times of 1 hour. The UV-treated substrates were then silanized by immersion in a gently stirred solution of 0.1% APTES in toluene for 1 hour, followed by rinsing with fresh toluene and drying with N_2. Curing of the silane linkages was carried out in an oven at 100 °C for 2 hours.

PAA was subsequently deposited onto the APTES-coated surfaces by spin coating solutions of 0.5-5.0 mg/ml PAA dissolved in methanol. Prior to the spin coating, each solution was filtered through a 0.2 µm Whatman® PFTE filter. Depending on the size of the substrate, 10-200 µL of solution was spread onto the substrate to fully cover the surface. Samples were spun at 2000 RPM for 120 seconds. In order to maximize coupling of PAA to the surface, the substrates were baked at 200 °C for 2 hours after spin coating to enhance amide formation between PAA carboxylic acid and APTES amine functional groups. Before use, the PAA-coated substrates were immersed in pH 8-10 buffer for 30 minutes to convert any newly formed anhydrides back to carboxylates.

Deposition of Lipid Bilayers

Lipid bilayers were deposited onto the PAA-coated substrate by employing LB/LS deposition or hybrid deposition using LB and vesicle fusion for the inner and the outer leaflets, respectively.[40] For reflectivity measurements, dDPPC membranes were formed at room temperature. For FRAP measurements, bilayers composed of DMPC containing 1 mol% Texas Red® DHPE fluorescent probe were formed at 18 °C. The DMPC membrane was deposited below its gel-fluid phase transition temperature (T_m = 24 °C) because gel phase bilayers are typically more conducive to transfer onto a substrate by LB/LS deposition. The LB/LS technique was performed using a Teflon® Langmuir–Blodgett trough (Nima, UK). Each PAA-coated substrate was first immersed in a subphase of MilliQ water, upon which a lipid monolayer was formed by spreading lipid, dissolved in chloroform, at the air-water interface. After spreading, the solvent was allowed to evaporate for a minimum of 15 minutes before the monolayer was compressed at a rate of 10–15 cm^2/min to a desired lateral pressure (45 mN/m for DPPC, 30 mN/m for DMPC). Once the desired surface pressure was achieved, the monolayer was equilibrated for at least 10 minutes. LB deposition onto the substrate was accomplished by raising the substrate vertically, oriented perpendicular to the surface of the subphase, through the air-water interface at a rate of 1 mm/min. After the substrate was fully removed from the subphase, the outer leaflet was deposited using LS deposition or vesicle fusion.

For LS deposition, the outer leaflet was transferred by lowering the inner leaflet coated substrate through the compressed lipid monolayer, this time oriented parallel to the air-water interface. Note that a faster dipping speed (10 mm/min) was used to prevent lipids from dispersing back onto the air-water interface. Once formed, the SLB was kept immersed in water. Using vesicle fusion, the SLB was formed by incubating the LB-deposited lipid monolayer with a freshly prepared solution of small unilamellar vesicles (SUVs) for 30 minutes. SUVs were made by drying a chloroform/lipid solution under a stream of N_2 and applying vacuum for at least 2 hours. Once dried, the lipids were resuspended in MilliQ water at a concentration of 1 mg/ml and probe tip sonicated to optical clarity to form a vesicle solution. Depending on the experiment, samples were either stored in buffer containing low (10 mM) or high (140 mM) concentration of monovalent salt (NaCl).

Fluorescence Recovery After Photobleaching (FRAP)

FRAP measurements were conducted on a Nikon Eclipse TE2000-S inverted fluorescence microscope (Technical Instruments, Burlingame, CA) equipped with two neutral density filters (ND8 and ND4), a Texas Red® filter set, and a Retige-1300 CCD camera (Technical Instruments). A mercury-vapor lamp filtered through the neutral density filter was used to illuminate the sample. Images were recorded through a Plan Fluor 10x objective (NA, 0.30) and processed using simple PCI software (Compix, Inc., Cranberry Township, PA). The sample was placed in a temperature controller on the microscope stage and held at 30 ± 1 °C (above the DMPC gel-phase transition temperature). Sample temperature was verified using a thermocouple fixed close to the region where the images were taken.

A standard FRAP measurement was performed by removing the neutral density filters and exposing a small spot with a high power beam through the Plan Fluor 40x objective (NA, 0.60) for 150 seconds, resulting in a circular 30 - 50 µm diameter bleached spot in the field of view. The fluorescence recovery process was then observed by recording an image of the entire field of view every 30 seconds through the Plan Fluor 10x objective (NA, 0.30). During this recovery period, the neutral density filters

were replaced to reduce further bleaching. The effective time-lapse video compiled from the acquired set of images was used to calculate the diffusion coefficient using the method described below.

Time-lapse videos were analyzed using a FRAP analysis program created in MATLAB (MathWorks, Natick, MA) by the Parikh research group and is described in detail elsewhere.[41] Basically, for each frame of the bleached spot, the program tracked parameters such as, location, width, and cross-sectional intensity to approximate the profile as a Gaussian function. Initial conditions extracted from the first post-bleached image were fit to a standard diffusion equation, Eq. 1. Analysis of subsequent frames produced a time-evolving Gaussian whose amplitude decayed as time increased as modeled by:

$$A(t) = \frac{C_0}{1+\frac{2Dt}{\sigma_0^2}} \qquad \text{[Eq. 1]}$$

Where *A(t)* is amplitude as a function of time, C_o is the initial amplitude, *t* is elapsed time, σ_o is the initial width of the Gaussian, and *D* is the diffusion coefficient.

Neutron Reflectivity

Reflectivity, *R*, is defined as the ratio of the number of particles (neutrons or photons) elastically and specularly scattered from a surface to that of the incident beam. When measured as a function of wave-vector transfer, $q_z = 4\pi \sin\theta/\lambda$, where ϑ is the angle of incidence and λ is the wavelength of the beam, the reflectivity curve contains information regarding the sample-normal profile of the in-plane averaged scattering length density (SLD) and is therefore most suited for studies of interfacial, layered films. The measured reflectivity curves were modeled using the Parratt formalism. The structural components of the system were divided into homogeneous molecular slabs or boxes of different scattering length density. These boxes, which physically represent different portions of the cushioned-membrane layers, were then refined using a least-squared method (Parratt 1954) to determine the thickness of each layer (box), scattering length density (β(z)), and adjacent interfacial roughness, enabling the structural components perpendicular to the interface to be resolved.[42-43] The model parameter optimization was carried out using the software package MIRROR developed by William A. Hamilton and

John B. Hayter, HFIR Center for Neutron Scattering, Condensed Matter Sciences Division, Oak Ridge National Laboratory.[45] A recent review provides a concise summary of neutron scattering characterization of lipid membranes.[46]

NR measurements were performed using the time-of-flight Surface Profile Analysis Reflectometer (SPEAR) at Manuel Lujan Jr. Neutron Scattering Center (Los Alamos National Laboratory, NM). The wavelengths of the neutrons were in the range of 4-16 Å, and the measured q_z range extended from $8x10^{-3}$ to 0.2 $Å^{-1}$. Specular reflectivities above noise level were obtained down to values of $R = 10^{-6}$. The experimental uncertainties were estimated by the neutron counting statistics (standard deviation, σR) with the experimental resolution in q_z being approximated by $\sigma q_z/q_z = 3\%$ for the measured q_z range.

Results and Discussion

Properties of Poly(Acrylic Acid) (PAA) Cushions

PAA is a polyelectrolyte composed of ionizable monomers of carboxylic acid (**Fig. 2.1**) and is available in a wide selection of molecular weights. The degree of ionization of the carboxylic acid groups (pKa = 4 – 4.5[47]) can be adjusted by varying the pH of the aqueous solution. Under alkaline conditions (pH > pKa) the majority of the PAA chains become deprotonated and the cushion gradually swells to 2–10 times its original, dry thickness. Under acidic conditions (pH < pKa), the PAA chains assume a predominantly protonated state and the cushion collapses.[22] As expected for an ideal polyelectrolyte, the process of protonation or deprotonation is reversible.[36-37] The PAA film can be easily cycled between the expanded and collapsed state by changing the pH of the imbibed solution.

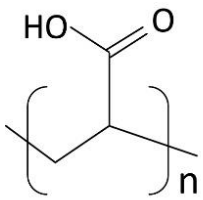

Fig. 2.1. Schematic of protonated poly(acrylic acid).

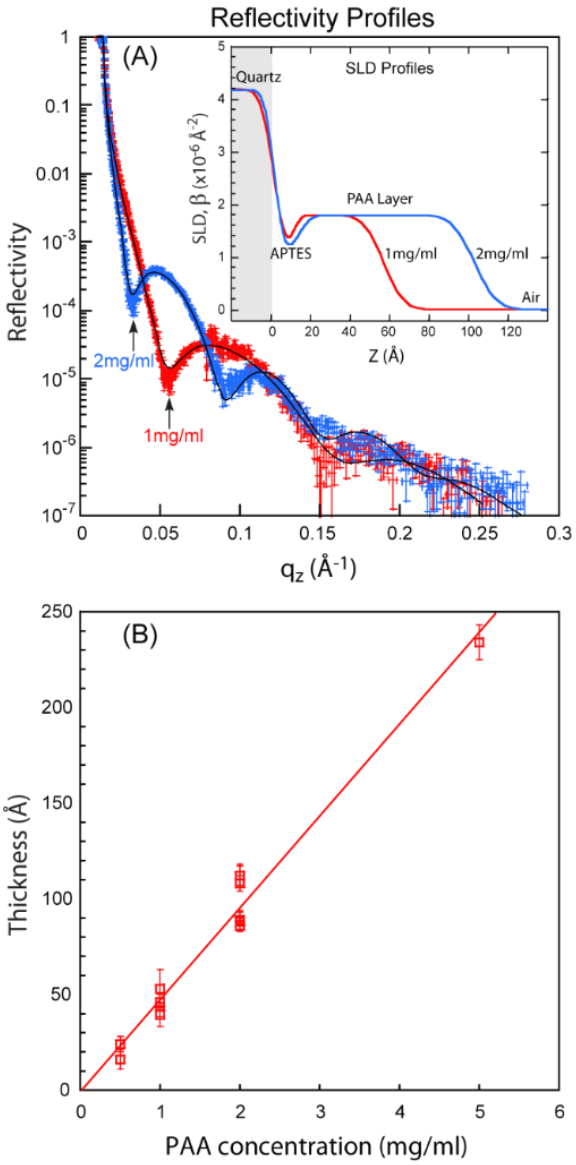

Fig. 2.2: (A) Reflectivity curves from typical 1 mg/ml PAA and 2 mg/ml PAA samples. Solid lines are fits to the data based on the SLD profiles shown in the inset. (B) Measured PAA film thickness as a function of PAA spin coating solution concentration. Error bars on data points are indicative of film roughness.

PAA Films in Air

Before use, the quality and thickness of the spin coated PAA films were characterized by NR. **Fig. 2.2 (A)** shows characteristic NR data for two PAA layers on planar quartz substrates in air. One was prepared using a 1 mg/ml PAA solution and the other from a 2 mg/ml PAA solution. Solid lines are least-squares fits corresponding to parameterized slab models shown in the inset. The fitted SLD of 1.5-1.7x10^{-}

^{6} Å for PAA in ambient conditions is in excellent agreement with the expected SLD of 1.69x10^{-6} Å based on the chemical composition of protonated PAA and its bulk mass density,[48] ρ_{dry} = 1.22 g/cm^3. The grafting density, σ, of the PAA chains in the cushion layer can be calculated from the measured values of PAA film thickness, d, according to Eq. 3,

$$\sigma = \frac{d\rho_{dryN_A}}{M_N} \qquad \text{[Eq. 3]}$$

where N_A denotes the number of molecules per mole and M_N = 450,000 Da, the PAA molecular weight. The APTES monolayer is visible as a dip in the SLD against the quartz surface. **Fig. 2.2 (B)** shows the measured PAA thickness as a function of spin coating solution concentration, ranging from 0.5-5 mg/ml PAA in methanol. Here, the roughness of the fitted PAA layer at the air-interface is indicated by the vertical extension of the error bars. The thickness of the PAA layer is shown to increase linearly with concentration of the spin coating solution.

PAA-Cushioned Membranes

The structure of PAA-cushioned SLBs was determined using NR. Measurements were sensitive to variations in nuclear density between categorical layers of the SLB including, the solid quartz substrate, the hydrated PAA cushion, the tail region of the lipid bilayer, and bulk water. SLBs were assembled using DPPC with deuterated lipid tails (dDPPC) to enhance signal contrast of the membrane relative to the PAA cushion and subphase. **Fig. 2.3 (A)** shows NR data (symbols) from a single dDPPC lipid bilayer, deposited by LB-LS at a lateral pressure of 45 mN/m on top of a PAA layer formed using a 2 mg/ml PAA spin coating solution. Solid lines are least-squares fits corresponding to parameterized slab models shown in **Fig. 2.3 (B).** Measurements were recorded under varied pH conditions, which were cycled sequentially from pH ~5.8 (MilliQ water) to pH 4, to pH 9, then back to pH 4. It was found that the PAA-cushioned SLB reflectivity data could be modeled well with a simple two layer system of PAA and the deuterated tail region. For example, at pH ~5.8 the thickness of the hydrated PAA and lipid tail region was 180 Å and 41 Å, respectively. Note that we do not attempt to relate boxes and sample layers directly since the PAA layer

and the inner headgroup region are described by one box only. To further minimize the parameter space, the SLD of the quartz, deuterated tail region, and water substrate were kept fixed. **Table 2.1** summarizes the box model parameters obtained by fitting the data with this modeling approach.

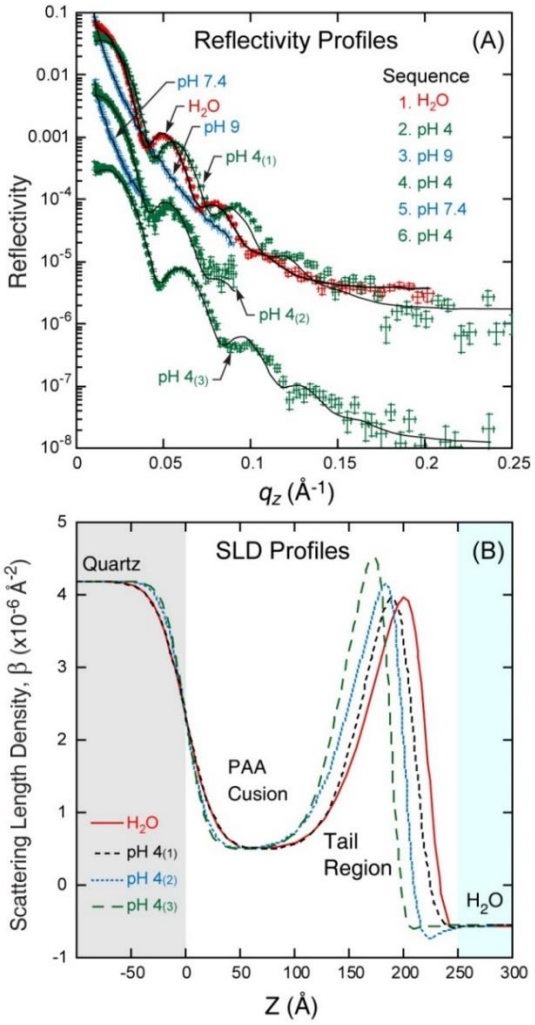

Fig. 2.3: (A) Reflectivity data from a dDPPC bilayer deposited on top of a PAA layer (2mg/ml) by LB/LS subjected to extensive cycling of pH conditions along with optimized model fits. Measurements at different pH conditions were performed sequentially as indicated in the key. (B) SLD profiles corresponding to the line fits shown in (A).

In the collapsed, low pH state, the fitted SLD of 0.5 ± 0.2 x10^{-6} Å^{-2} for the PAA layer was consistent with 33 to 55% hydration. Although the sensitivity to the absolute SLD/hydration state of the PAA layer is relatively modest, there is high sensitivity to the thickness of this layer. As a result, thickness changes of

the PAA layer from pH cycling are easily resolvable. The coverage of the dDPPC bilayer was estimated from the thickness of the deuterated tail region optimized against NR data describing the cushioned membrane when the PAA layer was collapsed (pH <6). Given the known volume of a 16-carbon lipid tail (860 $Å^3$) and the established area of DPPC lipids in the gel phase (46 $Å^2$), the ideal hydrocarbon tail layer thickness, d_{tail} = 2(860 $Å^3$)/46 $Å^2$ = 37 Å. The fitted SLD of the hydrocarbon tail region of 39 Å corresponds well with calculated values.[49] In effect, a well packed membrane covered 104 ± 10% of the PAA surface as calculated from both the model SLDs (here fixed to an SLD of 5.8x10^{-6} $Å^{-2}$ for fluid hydrocarbon) and the thickness of the deuterated tail region. The potentially greater than 100% coverage is consistent with the increased roughness of the membrane (~12 Å r.m.s.) compared to membranes supported directly on the quartz substrate (4-8 Å r.m.s) and the presence of gel-phase domains in the membrane.[50-53] Conversely, the SLD of a fully gel phase acyl chain region would be 20% higher.

Table 2.1: Box model fitting parameters for dDPPC on a PAA cushion formed using a 2 mg/mL spin coating solution.

Condition	PAA thickness (Å) ±4	PAA SLD (x10^{-6} $Å^{-2}$) ± 0.2	PAA r.m.s. roughness (Å) ±2	Tail region thickness (Å) ±2	Membrane r.m.s. roughness (Å) ±2	χ^2
H_2O	180	0.5	37	41	12	2.4
pH $4_{(1)}$	162	0.5	36	39	9	5.9
pH 9						
pH $4_{(2)}$	171	0.5	32	39	13	2.1
pH 7.4						
pH $4_{(3)}$	151	0.5	28	37	9	5.1

Fixed parameters: Substrate quartz SLD = 4.18x10^{-6} $Å^{-2}$, quartz roughness 3 Å, subphase H_2O SLD = -0.55x10^{-6} $Å^{-2}$, deuterated tail region SLD = 5.8x10^{-6} $Å^{-2}$. The SLD of the PAA film was allowed to vary.

Cycling of pH clearly demonstrated that the PAA cushion thickness was very sensitive to the environmental pH conditions. As can be seen in the reflectivity data and SLD model fits in **Fig. 2.3**, the PAA layer collapsed at lower pH conditions (pH 5.8 or 4.0). At higher pH conditions (pH 7.4 and pH 9) the PAA layer became negatively charged due to deprotonation and swelled substantially. Complementary ellipsometry and AFM measurements revealed that the PAA thickness increased by about a factor of five when going from pH 4 to pH 7.4.[22] This expansion was accompanied by an increase in interfacial roughness of the PAA cushion. At pH 7.4 and pH 9, the contrast between the hydrated, diffuse PAA-cushioned SLB and bulk water was reduced below detectable resolution. More specifically, the characteristic Kiessig fringes were not observed and the reflectivity profile appeared to be that of the Fresnel from the quartz-water interface. The coupling between the PAA cushion and the membrane is sufficient that the presence of the membrane is no longer detectable by neutron reflectivity due to roughness of the membrane interfacial layer. Importantly, the membrane remains contiguous at elevated pH as evidenced by FRAP measurements described later.

Consistent with membrane continuity, the SLB structure was preserved upon lowering the solution pH and re-collapse of the PAA cushion. Loss of material was only observed when the PAA films were not cured, likely because cured PAA films were more stably grafted to the underlying substrate via amide formation between the carboxylic acid groups in the PAA and the amine groups in the APTES layer.[54] The reversibility of the swelling process of the PAA cushion, including its effects on the lipid bilayer, was demonstrated by extended cycling of pH (pH $4_{(3)}$) shown in **Fig. 2.3**. Evidenced by the small decrease in hydrocarbon tail region thickness (**Table 2.1**), there was a minor reduction in the coverage of the lipid bilayer after pH cycling. This effect may have been due in part to the process of solvent exchange, which could have introduced air bubbles into the sample holder. Variation in the thickness of the deuterated tail region (SLD fixed to 5.8×10^{-6} Å^{-2}) cannot be decoupled from the slight differences in the roughness of the underlying PAA cushion in the collapsed state. At pH 4, small deviations in PAA thickness were likely

because of improved solvent exchange process. However, the decrease in cushion roughness may indicate that the PAA film becomes more uniform during the pH cycling process. Contrary to the alkaline conditions that resulted in weak coupling between the membrane and deprotonated PAA cushion, acidic conditions (pH 4) promoted strong attractive interactions between the membrane and the protonated cushion. This finding was consistent with the reduced diffusion coefficient of PAA-cushioned SLBs under acidic conditions as described later.

Hybrid LB/Vesicle Fusion of PAA-Cushioned Membranes

To investigate SLBs amenable to introduction of integral membrane proteins, we characterized PAA-cushioned membranes that were prepared using a hybrid approach of depositing the inner leaflet by LB and the outer leaflet, by vesicle fusion. Presumably, the SUVs here could be replaced by proteoliposomes [26] in derivative experiments. **Fig. 2.4 (A)** shows NR data from dDPPC lipid bilayers formed using this approach while **Fig. 2.4 (B)** shows the model SLDs corresponding to the least-squares fits. As expected, the thickness of the PAA layer formed with a 1 mg/ml spin coating solution was definitively smaller compared to that of the PAA layer formed with a 2 mg/ml spin coating solution. Based on the SLD profile of the deuterated lipid tail region, the surface coverage of the membrane formed by vesicle fusion deposition of the outer leaflet was approximately 10% less than that obtained using LS deposition. Still, the membrane coverage was quite high and membrane structure was retained throughout cycling of pH (results not shown). Ongoing studies now focus on optimization of deposition conditions and incorporation of proteins for high-resolution structural characterization.

Membrane Diffusion

DMPC self-diffusion coefficients in PAA-cushioned bilayers doped with 1 mol% Texas Red-DHPE prepared by LB/LS were determined as a function of pH and PAA film thickness. Control measurements of lipid diffusion on ultra-clean, UV-ozone treated glass supports without PAA (uncoated) are provided for comparison. The use of a quartz versus glass substrate was found to have negligible impact on diffusivity

measurements for both PAA-cushioned and non-cushioned membranes. For each SLB construction, FRAP was performed at multiple locations (minimum of 4) across the surface for over 10 unique samples to obtain the reported average diffusion coefficient. Differences in the background intensities in the figures are due to minor discrepancies in light intensity, optical alignment of the microscope, and sample characteristics during the time of the experiment.

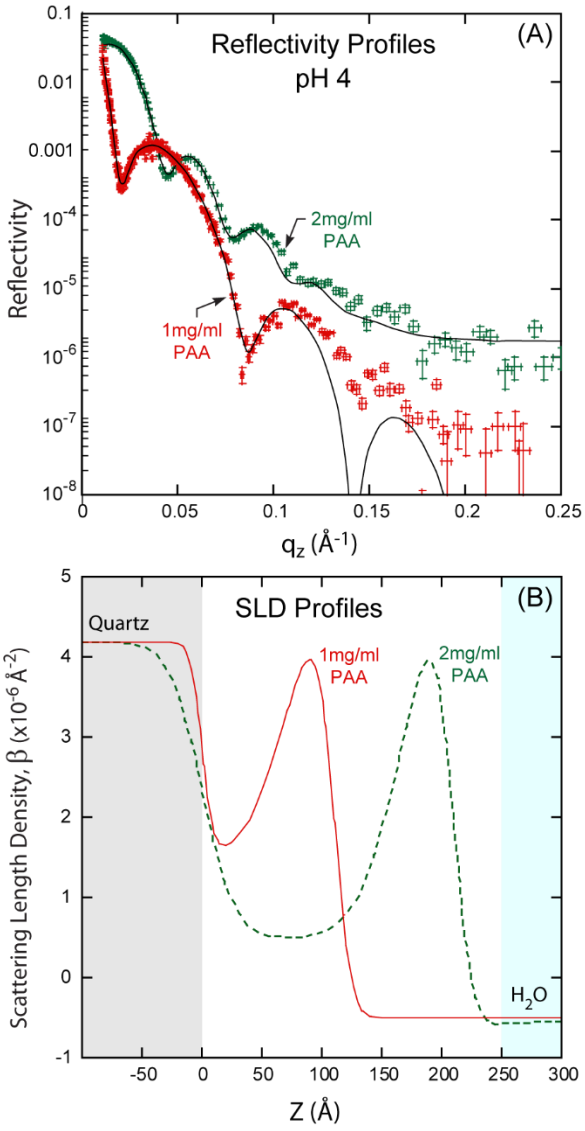

Fig. 2.4: (A) Reflectivity data from a dDPPC bilayer deposited on top of a 1 mg/ml and 2mg/ml PAA layer by LB (inner leaflet) and vesicle fusion (outer leaflet) at pH 4.0 along with optimized model fits. (B) SLD profiles corresponding to line fits shown in (A).

Influence of Initial PAA Thickness and pH on Diffusion

Results from two nominal PAA film thicknesses are reported using spin coating solutions comprised of 1 mg/ml and 2 mg/ml PAA in methanol. However, the diffusivity of lipids in PAA-cushioned SLBs was found to be unaffected by the starting, dry thickness of the PAA. Hence, the total thickness of the cushion can be liberally adjusted to meet the needs of different applications. Because the thickness of the polymer cushion could also be manipulated by pH, the dry thickness was adapted as a metric for distinguishing the effect of the total amount of PAA comprising the film. At pH 7.4, the diffusion coefficients of DMPC bilayers on PAA-coated glass substrates formed by 1 mg/ml and 2 mg/ml PAA solutions were 1.93 $\mu m^2/s \pm 0.55$ (N = 52) and 1.90 $\mu m^2/s \pm 0.86$ (N = 13), respectively. A representative FRAP image sequence is shown in **Fig. 2.5** and the summary of the diffusion coefficients is provided in **Table 2.2**.

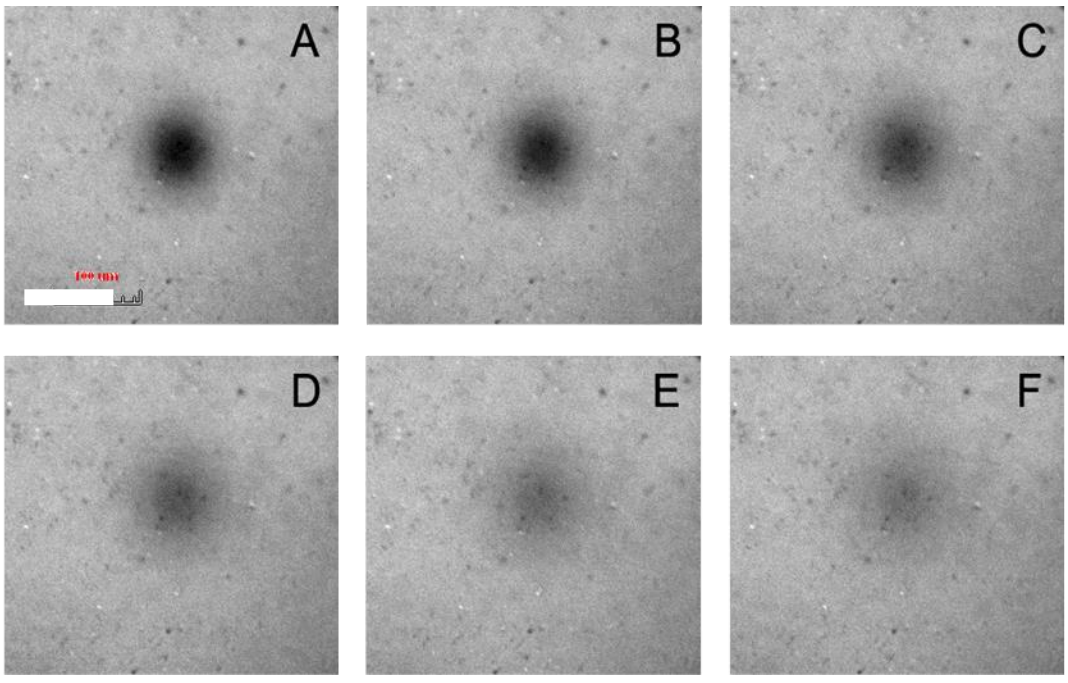

Fig. 2.5: FRAP measurements of DMPC doped with 1% Texas Red-DHPE on 1 mg/mL concentration of PAA coated glass substrate at pH 7.4. Image (A) was taken after 150 sec of photobleaching and the times elapsed from this point are (B) 30 sec, (C) 1 min 30 sec, (D) 3 min, (E) 4 min 30 sec, (F) 6 min. Scale bar is 100 µm.

Table 2.2: Diffusion coefficients of DMPC doped with 1 mol% Texas Red-DHPE on glass substrates, in 10 mM phosphate buffer adjusted to different pH conditions.

	Diffusion Coefficient [$\mu m^2/s$]		
pH	**1 mg/ml***	**2 mg/ml***	**no PAA**
9.2	2.64 ± 0.80	2.53 ± 0.78	2.39 ± 0.33
7.4	1.93 ± 0.55	1.90 ± 0.86	1.73 ± 0.44
4.0	0.12 ± 0.05	0.10 ± 0.02	1.71 ± 0.15

* Concentration of spin coating solution used to form the PAA film.

At 30 °C (above the gel-fluid phase transition temperature) in pH conditions where the polymer was swollen (pH 9.2 and 7.4), the diffusivity of SLBs formed on PAA-cushioned and un-cushioned substrates was between 1–3 $\mu m^2/s$. In contrast, the diffusivity of PAA-cushioned SLBs was reduced by more than an order of magnitude at pH 4. To interrogate the impact of the collapsed polymer cushion on lipid diffusion under acidic conditions (pH 4), the temperature of FRAP measurements was increased. Remarkably, heating the samples to 45 °C allowed the lipid bilayer to diffuse at a similar rate to what was observed at pH 9.2 or pH 7.4. In other words, the gel-fluid phase transition temperature of PAA-cushioned membranes appeared to be elevated at lower pH conditions. Since the pKa of the amine group in DMPC (pKa ~ ~7.9[i]) was above the pH of the bulk acidic solution, the phenomenon was unlikely attributed to changes in electrostatic charge of lipids in the membrane. Rather, elevation of the phase transition temperature most likely resulted from prominent coupling interactions between the bilayer and protonated PAA cushion.

Diffusion of PAA-Cushioned Membranes under Physiological Conditions

To test the behavior of PAA-cushioned SLBs under physiological saline conditions,[55] FRAP experiments were repeated in 140 mM NaCl and 10 mM pH 7.4 phosphate buffer on films produced using 1 mg/ml PAA solution. Qualitative observations from fluorescence microscopy images indicated that the PAA-cushioned bilayer had a homogeneous surface. The average diffusion coefficient was determined to be 1.92 $\mu m^2/s$ ± 0.56 (N = 17), which was comparable to values obtained in the lower ionic strength

conditions described earlier. Increasing the concentration of monovalent Na^+ ions had no discernable impact on the mobility of the lipid bilayer. This result was in good agreement with the conclusions of Jacobson and Papahadjopoulos,[56] who reported no appreciable effect of monovalent salt concentration on the phase transition temperature of electrically neutral PC bilayers.

Comparison to Reported Diffusion Coefficient Values

Reported diffusion coefficients for DMPC and DPPC bilayers on glass were factors of 1–2 higher (2–4 $\mu m^2/s$) [57], but on the same order of magnitude as values measured on glass substrates in this study. Not surprisingly, membranes supported by solid inorganic substrates typically exhibit slower diffusion rates when compared to analogous free-standing bilayers.[22] Improved mobility has been reported from polyelectrolyte-supported bilayers, which can sustain diffusion coefficients on the order of 10^{-3}-10 $\mu m^2/s$ when the polyelectrolyte is completely swollen in water.[58-59] Similarly in this work, lipids in the PAA-cushioned SLBs diffused slightly faster than lipids in membranes supported on UV-ozone treated glass. Moreover, lipid diffusivity could be arrested by reducing pH and driving the PAA into a collapsed state.

Conclusion

As demonstrated, PAA-cushioned membranes offer an easily tunable system for biophysical studies. The membrane-cushion interactions can be modulated by changing the pH of the bulk solution which, in turn, modulate membrane properties. The PAA cushion presents a reversible, convenient way to restrict the diffusion of lipids and membrane-associated molecules, even at temperatures above the canonical chain-melting phase transition temperature of the bilayer. Indeed, discordant results between experiments on polymer-cushioned SLBs found in the literature are likely due to the pronounced sensitivity of bilayer dynamics to subtle interactions with the cushion and solution conditions. The extensive findings presented here, based on structural characterization using NR and diffusion coefficient measurements using FRAP, highlight some important information for consideration. NR measurements showed that the dry thickness of the PAA layer can be precisely controlled by adjusting the concentration

of the spin coating solution. The degree of PAA cushion protonation and, therefore, the hydrated thickness of the cushion can be easily manipulated by adjusting solution pH conditions. At pH 5.8 and pH 4, the cushion is collapsed (protonated) and contains ~40% water. At pH 7.4 and pH 9.2, the cushion swells significantly (deprotonates) with an associated increase in roughness. Structural changes induced by pH cycling are reversible and the structure of the membrane is maintained during this process. While further in-depth studies are needed to assess long term membrane stability, both the PAA layer and the supported membrane were exceptionally stable, as measurements over the course of several days yielded similar results.

Diffusion experiments of PAA-cushioned SLBs showed that while altering the dry thickness of PAA did not affect the lipid diffusion coefficient, changes in pH can be used to stimulate emphatic, physical change in the membrane by modulating coupling of the bilayer to the polymer cushion. Namely, the lateral diffusion of lipids and membrane-associated molecules can be restricted by exposing PAA-cushioned SLBs to acidic conditions. The resulting stronger attractive interactions between the membrane and the collapsed, largely protonated PAA film effectively elevate the supported membrane's gel-fluid phase transition temperature. In summary, pH can be used to modify lipid diffusivity by altering the PAA cushion's three-dimensional structure and coupling of the membrane to the cushion. Furthermore, under physiological or alkaline conditions, lipids in PAA-cushioned membranes diffuse as fast as those in bilayers supported by bare, hydrophilic glass substrates.

Given their durable architecture and tractable diffusivity, PAA-cushioned membranes are a promising platform for closely mimicking a membrane in association with a cytoskeleton while accessing the advantages of a two-dimensional model membrane. High quality, high coverage membrane bilayers can be deposited on top of a PAA layer using both LB/LS and hybrid LB/vesicle fusion deposition methods. Overall, PAA-cushioned membranes seem well suited for exceedingly diverse applications including,

elucidation of membrane properties and membrane-protein interactions, as well as provide a framework for studying integral membrane proteins where the influence of the underlying support is minimized.

Acknowledgements

This work was supported by NSF Chemistry Division through grant CHE-1413745. We also thank William Chan for fluorescent microscopy measurements, and Gwen Schuman for her contributions in transfer ratio measurements.

References

1. Sackmann, E.; Tanaka, M., Supported membranes on soft polymer cushions: fabrication, characterization and applications. *Trends in biotechnology* **2000,** *18* (2), 58-64.
2. Sackmann, E., Supported membranes: Scientific and practical applications. *Science* **1996,** *271* (5245), 43-48.
3. McCabe, I. P., Forstner , Martin B., Polymer Supported Lipid Bilayers. *Open Journal of Biophysics* **2013,** *3* (1A), 59-69.
4. Diaz, A. J.; Albertorio, F.; Daniel, S.; Cremer, P. S., Double cushions preserve transmembrane protein mobility in supported bilayer systems. *Langmuir* **2008,** *24* (13), 6820-6826.
5. Tanaka, M.; Sackmann, E., Polymer-supported membranes as models of the cell surface. *Nature* **2005,** *437* (7059), 656-63.
6. Knoll, W.; Bender, K.; Förch, R.; Frank, C.; Götz, H.; Heibel, C.; Jenkins, T.; Jonas, U.; Kibrom, A.; Kügler, R., Polymer-Tethered Bimolecular Lipid Membranes. *Polymer Membranes/Biomembranes* **2010**, 87-111.
7. Andersson, J.; Köper, I., Tethered and Polymer Supported Bilayer Lipid Membranes: Structure and Function. *Membranes* **2016,** *6* (2), 30.
8. Spinke, J.; Yang, J.; Wolf, H.; Liley, M.; Ringsdorf, H.; Knoll, W., Polymer-supported bilayer on a solid substrate. *Biophysical journal* **1992,** *63* (6), 1667.
9. Wong, J. Y.; Majewski, J.; Seitz, M.; Park, C. K.; Israelachvili, J. N.; Smith, G. S., Polymer-cushioned bilayers. I. A structural study of various preparation methods using neutron reflectometry. *Biophys J* **1999,** *77* (3), 1445-1457.
10. Majewski, J.; Wong, J.; Park, C.; Seitz, M.; Israelachvili, J.; Smith, G., Structural studies of polymer-cushioned lipid bilayers. *Biophysical journal* **1998,** *75* (5), 2363-2367.
11. Baumgart, T.; Offenhausser, A., Polysaccharide-supported planar bilayer lipid model membranes. *Langmuir* **2003,** *19* (5), 1730-1737.
12. Smith, H. L.; Jablin, M. S.; Vidyasagar, A.; Saiz, J.; Watkins, E.; Toomey, R.; Hurd, A. J.; Majewski, J., Model lipid membranes on a tunable polymer cushion. *Physical review letters* **2009,** *102* (22), 228102.
13. Wang, L.; Schönhoff, M.; Möhwald, H., Lipids coupled to polyelectrolyte multilayers: ultraslow diffusion and the dynamics of electrostatic interactions. *The Journal of Physical Chemistry B* **2002,**

106 (35), 9135-9142.

14. Vockenroth, I. K.; Ohm, C.; Robertson, J. W. F.; McGillivray, D. J.; Losche, M.; Koper, I., Stable insulating tethered bilayer lipid membranes. *Biointerphases* **2008,** *3* (2), Fa68-Fa73.
15. Ma, Z.; Janmey, P. A.; Sharp, K. A.; Finkel, T. H., Improved method of preparation of supported planar lipid bilayers as artificial membranes for antigen presentation. *Microscopy research and technique* **2011,** *74* (12), 1174-85.
16. Mulligan, K.; Jakubek, Z. J.; Johnston, L. J., Supported Lipid Bilayers on Biocompatible Polysaccharide Multilayers. *Langmuir* **2011,** *27* (23), 14352-14359.
17. Goennenwein, S.; Tanaka, M.; Hu, B.; Moroder, L.; Sackmann, E., Functional incorporation of integrins into solid supported membranes on ultrathin films of cellulose: Impact on adhesion. *Biophysical Journal* **2003,** *85* (1), 646-655.
18. Tanaka, M.; Hermann, J.; Haase, I.; Fischer, M.; Boxer, S. G., Frictional Drag and Electrical Manipulation of Recombinant Proteins in Polymer-Supported Membranes. *Langmuir* **2007,** *23* (10), 5638-5644.
19. Jablin, M. S.; Dubey, M.; Zhernenkov, M.; Toomey, R.; Majewski, J., Influence of Lipid Membrane Rigidity on Properties of Supporting Polymer. *Biophysical Journal* **2011,** *101* (1), 128-133.
20. Smith, H. L.; Jablin, M. S.; Vidyasagar, A.; Saiz, J.; Watkins, E.; Toomey, R.; Hurd, A. J.; Majewski, J., Model Lipid Membranes on a Tunable Polymer Cushion. *Phys Rev Lett* **2009,** *102* (22).
21. Cassier, T.; Sinner, A.; Offenhauser, A.; Mohwald, H., Homogeneity, electrical resistivity and lateral diffusion of lipid bilayers coupled to polyelectrolyte multilayers. *Colloid Surf. B-Biointerfaces* **1999,** *15* (3-4), 215-225.
22. El-Khouri, R. J.; Bricarello, D. A.; Watkins, E. B.; Kim, C. Y.; Miller, C. E.; Patten, T. E.; Parikh, A. N.; Kuhl, T. L., pH Responsive Polymer Cushions for Probing Membrane Environment Interactions. *Nano Lett* **2011,** *11* (5), 2169-2172.
23. Blakeston, A. C.; Alswieleh, A. M.; Heath, G. R.; Roth, J. S.; Bao, P.; Cheng, N.; Armes, S. P.; Leggett, G. J.; Bushby, R. J.; Evans, S. D., New Poly(amino acid methacrylate) Brush Supports the Formation of Well-Defined Lipid Membranes. *Langmuir* **2015,** *31* (12), 3668-3677.
24. Singh, S.; Junghans, A.; Tian, J.; Dubey, M.; Gnanakaran, S.; Chlistunoff, J.; Majewski, J., Polyelectrolyte multilayers as a platform for pH-responsive lipid bilayers. *Soft Matter* **2013,** *9* (37), 8938-8948.
25. Watkins, E. B.; El-Khouri, R. J.; Miller, C. E.; Seaby, B. G.; Majewski, J.; Marques, C. M.; Kuhl, T. L., Structure and Thermodynamics of Lipid Bilayers on Polyethylene Glycol Cushions: Fact and Fiction of PEG Cushioned Membranes. *Langmuir* **2011,** *27* (22), 13618-13628.
26. Pace, H.; Simonsson Nyström, L.; Gunnarsson, A.; Eck, E.; Monson, C.; Geschwindner, S.; Snijder, A.; Höök, F., Preserved Transmembrane Protein Mobility in Polymer-Supported Lipid Bilayers Derived from Cell Membranes. *Analytical chemistry* **2015,** *87* (18), 9194-9203.
27. Naumann, C. A.; Prucker, O.; Lehmann, T.; Rühe, J.; Knoll, W.; Frank, C. W., The polymer-supported phospholipid bilayer: tethering as a new approach to substrate-membrane stabilization. *Biomacromolecules* **2002,** *3* (1), 27-35.
28. Wagner, M. L.; Tamm, L. K., Tethered Polymer-Supported Planar Lipid Bilayers for Reconstitution of Integral Membrane Proteins: Silane-Polyethyleneglycol-Lipid as a Cushion and Covalent Linker. *Biophysical Journal* **2000,** *79* (3), 1400-1414.

29. Junghans, A.; Koper, I., Structural Analysis of Tethered Bilayer Lipid Membranes. *Langmuir* **2010,** *26* (13), 11035-11040.
30. Reich, C.; Andruzzi, L., Preparation of fluid tethered lipid bilayers on poly(ethylene glycol) by spin-coating. *Soft Matter* **2010,** *6* (3), 493-500.
31. Beyer, D.; Elender, G.; Knoll, W.; Kuhner, M.; Maus, S.; Ringsdorf, H.; Sackmann, E., Influence of anchor lipids on the homogeneity and mobility of lipid bilayers on thin polymer films. *Angew Chem Int Edit* **1996,** *35* (15), 1682-1685.
32. Sinner, E. K.; Knoll, W., Functional tethered membranes. *Current opinion in chemical biology* **2001,** *5* (6), 705-711.
33. Fletcher, D. A.; Mullins, R. D., Cell mechanics and the cytoskeleton. *Nature* **2010,** *463* (7280), 485-492.
34. Liu, A. P.; Richmond, D. L.; Maibaum, L.; Pronk, S.; Geissler, P. L.; Fletcher, D. A., Membrane-induced bundling of actin filaments. *Nature physics* **2008,** *4*, 789-793.
35. Seitz, M.; Park, C. K.; Wong, J. Y.; Israelachvili, J. N., Long-Range Interaction Forces between Polymer-Supported Lipid Bilayer Membranes. *Langmuir : the ACS journal of surfaces and colloids* **2001,** *17* (15), 4616-4626.
36. Horkay, F.; Basser, P. J., Ionic and pH effects on the osmotic properties and structure of polyelectrolyte gels. *Journal of polymer science. Part B, Polymer physics* **2008,** *46* (24), 2803-2810.
37. Weidman, J. L.; Mulvenna, R. A.; Boudouris, B. W.; Phillip, W. A., Unusually Stable Hysteresis in the pH-Response of Poly(Acrylic Acid) Brushes Confined within Nanoporous Block Polymer Thin Films. *Journal of the American Chemical Society* **2016,** *138* (22), 7030-7039.
38. Welch, M. E.; Ober, C. K., Responsive and patterned polymer brushes. *Journal of Polymer Science Part B-Polymer Physics* **2013,** *51* (20), 1457-1472.
39. Blumenthal, D.; Goldstien, L.; Edidin, M.; Gheber, L. A., Universal Approach to FRAP Analysis of Arbitrary Bleaching Patterns. **2015,** *5*, 11655.
40. Kurniawan, J.; Ventrici de Souza, J. F.; Dang, A. T.; Liu, G.-y.; Kuhl, T. L., Preparation and Characterization of Solid-Supported Lipid Bilayers Formed by Langmuir–Blodgett Deposition: A Tutorial. *Langmuir* **2018,** *34* (51), 15622-15639.
41. Sanii, B.; Smith, A. M.; Butti, R.; Brozell, A. M.; Parikh, A. N., Bending membranes on demand: Fluid phospholipid bilayers on topographically deformable substrates. *Nano Lett* **2008,** *8* (3), 866-871.
42. Parratt, L. G., Surface Studies of Solids by Total Reflection of X-Rays. *Phys Rev* **1954,** *95* (2), 359-369.
43. Singh, S.; Junghans, A.; Waltman, M. J.; Nagy, A.; Iyer, R.; Majewski, J., Neutron reflectometry characterization of PEI-PSS polyelectrolyte multilayers for cell culture. *Soft Matter* **2012,** *8* (45), 11484-11491.
44. Als-Nielsen, J.; McMorrow, D., *Elements of modern X-ray physics*. Wiley: New York, 2001; p xi, 318 p.
45. The statistical and error estimation concepts used therein are described in: Bevington, P. R. Data Reduction and Error Analysis for the Physical Sciences; McGraw-Hill: New York, 1969; Chapter 11 and in: Press, W. H.; Teukolsky, S. A.; Vetterling, W. T.; Flannery, B. P. Numerical Recipes in Pascal; Cambridge University Press: Cambridge, 1989; Chapter 15. The minimization routine employed by the MIRROR program is the “downhill simplex” method: Nelder, J. A.; Mead, R. Comput. J. 1965,

7, 308 in an implementation described in Chapter 104 of Numerical Recipes.
46. Fragneto, G.; Delhom, R.; Joly, L.; Scoppola, E., Neutrons and model membranes: Moving towards complexity. *Current Opinion in Colloid & Interface Science* **2018,** *38*, 108-121.
47. Pradip; Maltesh, C.; Somasundaran, P.; Kulkarni, R. A.; Gundiah, S., Polymer-Polymer Complexation in Dilute Aqueous-Solutions - Poly(Acrylic Acid)-Poly(Ethylene Oxide) and Poly(Acrylic Acid)-Poly(Vinylpyrrolidone). *Langmuir* **1991,** *7* (10), 2108-2111.
48. Welsh, W., Physical Properties of Polymers Handbook. AIP Press Woodbury, NY: 1996.
49. Watkins, E.; Miller, C.; Mulder, D.; Kuhl, T.; Majewski, J., Structure and orientational texture of self-organizing lipid bilayers. *Physical review letters* **2009,** *102* (23), 238101.
50. Rondelli, V.; Del Favero, E.; Brocca, P.; Fragneto, G.; Trapp, M.; Mauri, L.; Ciampa, M. G.; Romani, G.; Braun, C. J.; Winterstein, L.; Schroeder, I.; Thiel, G.; Moroni, A.; Cantu, L., Directional K(+) channel insertion in a single phospholipid bilayer: Neutron reflectometry and electrophysiology in the joint exploration of a model membrane functional platform. *Biochimica et biophysica acta. General subjects* **2018,** *1862* (8), 1742-1750.
51. de Ghellinck, A.; Shen, C.; Fragneto, G.; Klosgen, B., Probing the position of resveratrol in lipid bilayers: A neutron reflectivity study. *Colloids and surfaces. B, Biointerfaces* **2015,** *134*, 65-72.
52. Smith, H. L.; Howland, M. C.; Szmodis, A. W.; Li, Q.; Daemen, L. L.; Parikh, A. N.; Majewski, J., Early stages of oxidative stress-induced membrane permeabilization: a neutron reflectometry study. *J Am Chem Soc* **2009,** *131* (10), 3631-8.
53. Krueger, S.; Koenig, B. W.; Orts, W. J.; Berk, N. F.; Majkrzak, C. F.; Gawrisch, K., Neutron reflectivity studies of single lipid bilayers supported on planar substrates. *Basic life sciences* **1996,** *64*, 205-13.
54. Zabicky, J., *The chemistry of amides*. Interscience Publishers/John Wiley & Sons: New York: 1970; Vol. 1.
55. Tamm, L. K.; McConnell, H. M., Supported phospholipid bilayers. *Biophysical Journal* **1985,** *47* (1), 105-113.
56. Jacobson, K.; Papahadjopoulos, D., Phase transitions and phase separations in phospholipid membranes induced by changes in temperature, pH, and concentration of bivalent cations. *Biochemistry* **1975,** *14* (1), 152-61.
57. Scomparin, C.; Lecuyer, S.; Ferreira, M.; Charitat, T.; Tinland, B., Diffusion in supported lipid bilayers: influence of substrate and preparation technique on the internal dynamics. *The European physical journal. E, Soft matter* **2009,** *28* (2), 211-20.
58. Fischlechner, M.; Zaulig, M.; Meyer, S.; Estrela-Lopis, I.; Cuellar, L.; Irigoyen, J.; Pescador, P.; Brumen, M.; Messner, P.; Moya, S.; Donath, E., Lipid layers on polyelectrolyte multilayer supports. *Soft Matter* **2008,** *4* (11), 2245-2258.
59. Smith, E. A.; Coym, J. W.; Cowell, S. M.; Tokimoto, T.; Hruby, V. J.; Yamamura, H. I.; Wirth, M. J., Lipid Bilayers on Polyacrylamide Brushes for Inclusion of Membrane Proteins. *Langmuir : the ACS journal of surfaces and colloids* **2005,** *21* (21), 9644-9650.

Chapter 3: Lipid and Protein Transfer between Nanolipoprotein Particles and Supported Lipid Bilayers

Amanda T. Dang[†], Wei He[‡], Daniela B. Ivey[#], Matthew A. Coleman[‡], and Tonya L. Kuhl[*#]

[†]Department of Materials Science and Engineering, University of California, Davis CA 95616
[‡]Lawrence Livermore National Laboratory, Livermore, CA 94550
[#]Department of Chemical Engineering, University of California, Davis CA 95616

Publication Status: Submitted and awaiting peer review

Keywords: nanolipoprotein particle, supported lipid bilayer, atomic force microscopy, apolipoprotein, membrane scaffold protein

Abstract: A nanolipoprotein particle (NLP) is a lipid bilayer disc stabilized by two amphipathic "scaffold" apolipoproteins. It has been most notably utilized as a tool for solubilizing a variety of membrane proteins while preserving structural and functional properties. Transfer of functional proteins from NLPs into model membrane systems such as supported lipid bilayers (SLBs) would enable new opportunities for example: Two-dimensional protein crystallization and studies on protein-protein interactions. This work used fluorescence microscopy (FM) and atomic force microscopy (AFM) to investigate the interaction between NLPs and SLBs. When incubated with SLBs, NLPs were found to spontaneously deliver lipid and protein cargo. The impact of membrane composition on lipid exchange was explored, revealing a positive correlation between the magnitude of lipid transfer and concentration of defects in the target SLB. Incorporation of lipids capable of binding specifically to polyhistidine tags encoded into the apolipoproteins also boosted transfer of NLP cargo. Optimal conditions for lipid and protein delivery from NLPs to SLBs are proposed based on interaction mechanisms.

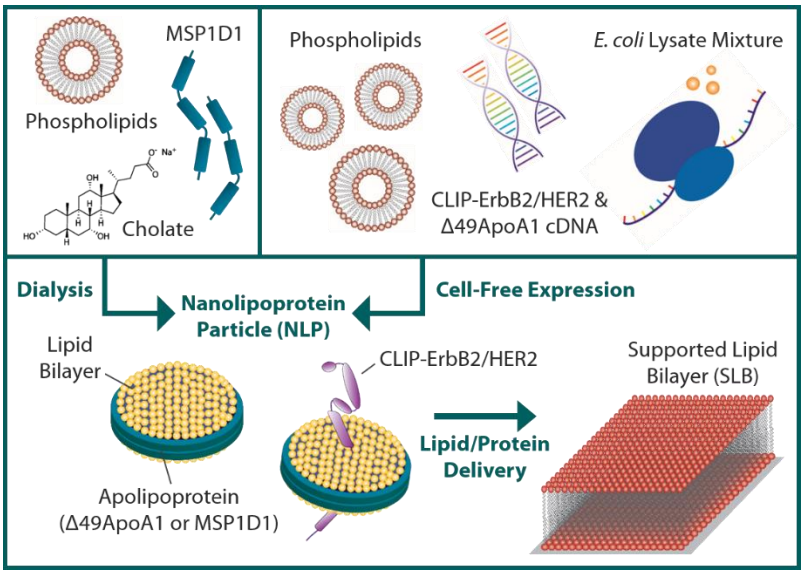

Introduction

Over the past two decades, the biomimetic nanolipoprotein particle (NLP) a.k.a. nanodisc[1] or reconstituted high-density lipoprotein (HDL) particle, has been steadily developed as a promising drug delivery vehicle[2-3] as well as a proficient tool for the expression and characterization of assorted membrane proteins.[4-6] Biocompatible and amenable to modification for enhanced serum stability,[7] NLPs emulate naturally occurring HDL particles, which transport lipidic cargo in the circulatory system.[8-9] HDL particles are soluble lipoprotein complexes with cores comprised of triglycerides, cholesterol esters, and cholesterols, encapsulated by a phospholipid bilayer and secured by amphipathic apolipoproteins.[10] Apolipoproteins mediate interactions with plasma membrane surface receptors and enable delivery of cholesterol via selective cellular uptake pathways.[8, 11-12] Additionally, they act as "scaffold" proteins that control particle size and structure.

In distinction from their biological HDL counterparts, ApoA1-based NLPs are discoidal lipid bilayers with an average thickness of 5 nm and diameters that range between 10 - 30 nm depending on the specific apolipoprotein and its ratio compared to lipids.[4, 13-15] Each ApoA1-based NLP has two apolipoproteins that insulate the hydrophobic core and dictate particle size. There are two popular methods for assembling NLPs *in vitro*. The first is reconstitution of apolipoprotein in the presence of lipids (vesicles) and detergent,[1, 16-17] where gradual dilution of the detergent induces self-assembly of NLPs. The second is cell-free expression of apolipoprotein in the presence of lipids. Importantly, the NLP assembly techniques result in production of identical nanoparticles.[14] Since the apolipoprotein can be made to encode a polyhistidine tag, NLPs can be purified using straightforward affinity chromatography procedures. The principle

advantage of cell-free expression is its capacity for simultaneous production of apolipoproteins and membrane proteins without the need for adding or removing detergents.[4] When co-expressed with NLPs, membrane proteins have been found to insert into NLP bilayers to form a stably solubilized membrane protein-NLP complexes (MP-NLPs). Importantly, membrane proteins in MP-NLP complexes have been shown to retain their structure and functionality using the "One-Pot" cell-free approach.[5, 18]

MP-NLP complexes have potential for broad utility in pharmaceuticals applications and in fundamental research on protein-protein and protein-lipid interactions. While strategies for preparation and characterization of proteins using high spatial resolution analytical techniques such as electron microscopy and X-ray crystallography have steadily improved, the crucial task of examining protein structure and functionality in native lipid environments remains a persistent challenge.[19] Even though membrane proteins make up over 60% of drug targets,[20] less than 1% of solved protein crystal structures are membrane proteins.[21] This is compelling motivation for development of broadly applicable, lipid-based characterization platforms, especially amid growing evidence that lipids not only stabilize,[22] but regulate membrane protein activity.[23-24] MP-NLPs offer one modality for examining properties of membrane proteins embedded in lipid bilayers. Several studies using NLPs to examine protein activity, [25] oligomerization,[26-27] and diffusion dynamics[18, 28] have been reported.

Another platform that recapitulates physicochemical properties of native membranes is the supported lipid bilayer (SLB). Similar to NLPs, SLBs are powerful tools for studying membrane proteins because they allow for observation of protein-lipid interactions,[24, 29] protein-protein interactions,[30] conformational changes, and hydrophobic mismatch with high fidelity.[31] A SLB is

a lipid bilayer that has been reconstituted on a solid, normally planar substrate such as silica or mica.[32] SLBs are generally more robust than freestanding bilayers. Further, SLBs are compatible with two-dimensional characterization methods including wide-field fluorescence microscopy (FM), electron microscopy, atomic force microscopy (AFM), and neutron or X-ray scattering. In addition, SLB lipid composition can be precisely tailored to simulate nano- to microscopic phase separation and lipid raft domains.[33] For studies on membrane proteins, SLBs can be modified with polymer cushions[34-36] to prevent unwanted interactions between embedded proteins and the underlying substrate. SLBs can also be micropatterned[37] to manipulate the spatial organization of associated molecules.

Mechanisms by which NLPs transfer lipids and proteins to and from other lipid constructs have been explored with bicelles[27, 38] and with other NLPs,[39] but scarcely with continuous bilayers. A recent study by Patriarchi et al.[40] showed that NLPs could deliver functional β_2-adrenergic receptor, a G-protein coupled receptor (GPCR), into the plasma membrane of living cells. However, the underlying mechanism behind the protein transfer process remains obscure. In this work, we used wide-field FM and AFM to determine the impacts of composition and the presence of defects on lipid cargo transfer from NLPs to SLBs.

Materials and Methods

General Materials and Methods

MilliQ deionized water (resistivity ≥18 MΩ·cm) from a Barnstead water purification system (Thermo Fisher Scientific) was used in all protocols except cell-free expression, which utilized DNA-ase free water included in the Invitrogen Expressway Maxi kit. The lipids 1,2-dimyristoleoyl-sn-glycero-3-phosphocholine (DMPC), 1,2-dipalmitoyl-sn-glycerol-3-

Phosphatidylcholine (DPPC), 1,2-dipalmitoyl-sn-glycero-3-phosphoethanolamine (DPPE), 1,2-dioleoyl-sn-glycero-3-phosphocholine (DOPC), 1,2-dioleoyl-sn-glycero-3-[(N-(5-amino-1-carboxypentyl)iminodiacetic acid)succinyl] (nickel salt) (DOGS-NTA-Ni), and 1,2-dipalmitoyl-sn-glycero-3-phosphoethanolamine-N-(lissamine rhodamine B sulfonyl) (ammonium salt) (Rhodamine-DHPE) were purchased from Avanti Polar Lipids, Inc. Texas Red™ 1,2-Dihexadecanoyl-sn-Glycero-3-Phosphoethanolamine, Triethylammonium Salt (TR-DHPE) and Oregon Green™ 488 1,2-dihexadecanoyl-sn-glycero-3-phosphoethanolamine (OG-DHPE) labeled lipid reagents were purchased from Thermo Fisher Scientific. Lipids were dissolved in Chloroform, HPLC grade (Thermo Fisher Scientific) to make solutions at a concentration of 1 mg/ml. Sodium chloride (≥ 99% purity), imidazole (≥ 99% purity), Trizma® hydrochloride and Trizma® base were used to prepare pH 7.4 Tris buffer. Sodium cholate hydrate (≥ 99% purity) was purchased from Sigma-Aldrich, Inc. Phosphate buffered saline (PBS) dry pack, ultra-pure grade, was purchased from Apex Bioresearch, Inc. and dissolved in MilliQ deionized water to make PBS buffer (10 mM phosphate buffer, 137 mM NaCl, 2.7 mM KCl).

Glass coverslips (Thermo Fisher Scientific) were cleaned with Hellmanex basic detergent (Sigma-Aldrich), rinsed with MilliQ deionized water followed by 200 proof ethanol, and dried under a stream of nitrogen (specialty grade, 99.998% pure). Lastly, glass substrates were UV-ozone treated to promote hydroxyl group formation at the surface and used within 30 min of treatment. Coverslips functionalized with poly(acrylic acid) (PAA) cushions were additionally subjected to sonication in acetone, then isopropyl alcohol to ensure full removal of organic contaminants from the surface prior to UV-ozone treatment and PAA deposition. Mica (Axim Mica) was freshly cleaved before use.

PAA Cushion Preparation

PAA cushions were prepared using spin-coating methods previously described by El-Khouri et al.[34] Basically, deposition solutions were prepared by dissolving PAA (450k MW, 0.1% cross-linked, Sigma-Aldrich, Inc.) in methanol (≥ 99% purity, Sigma-Aldrich**)** at a concentration of 1 mg/mL. To enable covalent grafting of polymer chains to the silica substrate, coverslip surfaces were initially functionalized with aminopropyltriethoxysilane (APTES, Gelest, Inc.) by solution deposition in toluene (≥ 99% purity, Sigma-Aldrich). The PAA cushion was then formed by spin-coating and subsequent curing. Finally, PAA substrates were immersed in Tris buffer (pH 9) to convert anhydrides to carboxylates and relieve mechanical stresses in the polymer layer. As previously reported,[34] cushion thickness can be modified by altering the concentration of the PAA in the spin-coating solution. The technique of UV-Ozone photolithography was used to pattern PAA cushions into arrays of 100 – 200 µm squares. Areas exposed during photolithography were subsequently treated with AquaSil siliconizing fluid (Thermo Fisher Scientific) to render them resistant to nonspecific protein adsorption. Additional details for PAA-cushion preparation is provided in the Supporting Information.

SLB Sample Preparation

SLBs were deposited on bare glass coverslips (Thermo Fisher Scientific) or freshly cleaved mica (Axim Mica) using vesicle fusion, Langmuir-Blodgett (LB)-LB deposition, or LB-Langmuir-Schaeffer (LS) deposition. In LB-LB deposition, each leaflet was added by moving the substrate vertically through a compressed lipid monolayer at an air-water interface. In LB-LS deposition, the outer leaflet was transferred by lowering the substrate through the air-water interface

oriented parallel to the monolayer.[32, 41] Details on methods used to produce each SLB are summarized in **Table 3.S1** in Supporting Information.

Vesicle Sample Preparation

Vesicle solutions for comparative lipid exchange experiments were prepared by sonication. A mixture of DMPC containing 2 mol% Rhodamine-DHPE was dissolved in chloroform, dried under nitrogen, and placed under vacuum for at least 4 h. The mixture was hydrated with PBS buffer to a concentration of 0.1 mg/mL, vortexed for 15 sec, and then placed in an ultrasonic bath sonicator for 30 min. Vesicle solutions were always used within 1 hour after preparation. Size determination by dynamic light scattering (DLS, Malvern Zeta Sizer) revealed an average vesicle size of 55.5 ± 11 nm in diameter.

NLP Assembly from Lyophilized Apolipoprotein

The NLPs stabilized with membrane scaffold protein MSP1D1 (MSP1D1-NLPs) were assembled using methods adopted from the process described by Zeno et al.[42] In brief, a stoichiometric excess of DMPC doped with 2 mol% Rhodamine-DHPE was dried in a glass vial with nitrogen and placed under mild vacuum for at least 6 hr. The lipid mixture was then hydrated in Tris buffer containing sodium cholate hydrate and added to another aliquot of Tris buffer containing MSP1D1. Each MSP1D1 had a chain length of 217 amino acids (25.3 kDa) and a polyhistidine tag attached to its N-terminus. After incubation, the mixture was transferred to a 10 kDa MWCO Slide-A-Lyzer dialysis cassette (Thermo Fisher Scientific) and dialyzed at 4 °C, in Tris buffer (pH 7.4) to promote cholate removal and NLP assembly. Subsequent purification (described below) ensured complete cholate removal from the final product. For the detailed protocol for synthesis of MSP1D1-NLPs, see Supporting Information.

NLP Assembly using Cell-Free Expression

The NLPs stabilized with apolipoprotein Δ49ApoA1 (Δ49ApoA1-NLPs) and with embedded receptor tyrosine kinase CLIP-ErbB2/HER2 (CLIP-ErbB2-NLPs) were prepared using cell-free expression methods described by He et al.[5] The cell-free reaction was carried out using the Invitrogen Expressway™ Maxi Cell-Free *E. coli* Expression System (Thermo Fisher Scientific). Plasmids encoding CLIP-ErbB2/HER2 and a truncated 6xHis-tagged version of human apolipoprotein A-I, missing the amino-terminal 49 amino acids (Δ49ApoA1) were codon optimized for *E. coli* expression.[5] Δ49ApoA1-NLPs were assembled with DMPC vesicles containing 0.5 mol% TR-DHPE. CLIP-ErbB2 NLPs were conjugated with fluorescent substrate CLIP-Cell TMR-Star (New England Biolabs), added to the cell-free reaction 1 hr prior to purification.

NLP Purification and Verification

All NLPs were isolated by nickel affinity purification. Initially, samples were incubated for 1 hr with HisPur™ Ni-NTA resin (Thermo Fisher Scientific), rinsed with Tris buffer (pH 7.4) at 4°C. Next, 3-4 wash steps were then performed using Tris buffer containing 20 mM imidazole, followed by 3-4 elution steps with Tris buffer containing 400 mM imidazole. NLPs in the eluted fraction were concentrated using a Vivaspin 100 kDa MWCO centrifugal concentrator[13] (Thermo Fisher Scientific). To remove imidazole from the solution, concentrated samples were transferred to 10 kDa MWCO Slide-A-Lyzer dialysis cassettes (Thermo Fisher Scientific) and dialyzed at 4 °C, in PBS buffer (pH 7.4) at over 500 times the sample volume (4 buffer exchanges over 36 hours). Recovered samples were stored in the dark at 4 °C until use.

Production of MSP1D1, Δ49ApoA1, and CLIP-ErbB2/HER2 protein particles was verified by SDS-PAGE. Protein concentration in each sample was adjusted to 0.1 mg/mL and verified by

measuring peak absorbance at 280 nm using a UV-vis spectrophotometer (Shimadzu Scientific Instruments). The average discoidal diameter of MSP1D1-NLPs, determined by DLS (Malvern Zeta Sizer), was 20.7 ± 1.6 nm and comparable to sizes reported for Δ49ApoA1-NLPs[4] and CLIP-ErbB2-NLPs.[5] Additional details on NLP verification are included in the Supporting Information.

NLP Incubation with SLBs

At the start of each incubation step, 50 µL of 0.1 mg/mL NLP solution was pipetted into a 3 mL volume of PBS buffer containing the SLB (final NLP concentration ~1.6 µg/mL). At the end of each incubation period, residual NLPs or vesicles were removed by exchanging the incubation solution covering the SLB with fresh buffer. Total incubation time was varied to suit the unique conditions of each experiment. For example, in FM measurements, MSP1D1-NLPs and Δ49ApoA1-NLPs were incubated with glass-supported bilayers for 15 min and PAA-cushioned SLBs for 30 min, respectively. However, CLIP-ErbB2-NLPs were incubated for 12 hr with PAA-cushioned SLBs because earlier trials (unpublished data) indicated that at least several hours were required to accumulate enough protein in the SLB to produce an appreciable fluorescent signal. For lengthier AFM experiments, Δ49ApoA1-NLPs were also incubated for 12 hr with SLBs. The extended duration was necessary to assure the samples had reached static equilibrium before the start of topography scans.

Fluorescence Microscopy

The FM images were acquired using a Nikon Eclipse E600 microscope connected to an Andor Zyla sCMOS camera (DG-152V-C1E-FI) at 40X magnification. A mercury short-arc lamp (Osram, HBO 100W/2) was used to illuminate samples. A TRITC filter cube (dichroic cut-on wavelength 562 nm), TR filter cube (dichroic cut-on wavelength 593 nm), and FITC filter cube

(dichroic cut-on wavelength 506 nm) were used to isolate fluorescence emission from Rhodamine-DHPE/CLIP-Cell TMR-Star, TR-DHPE, and OG-DHPE, respectively. For mean fluorescence intensity measurements, at least 10 images were recorded across the surface of each sample and analyzed using a MATLAB program (see Supporting Information for details).

Atomic Force Microscopy

AFM images were acquired in PBS buffer using a MFP3D-SA system (Asylum Research, Santa Barbara, CA) equipped with a medium soft silicon cantilever (model AC240TS-R3, Asylum Research, Santa Barbara, CA) with a spring constant of 2 N/m. Images were recorded in tapping mode AFM with a set point of 250-300 mV and a scan rate of 1.5 Hz. AFM images were analyzed using Gwyddion ver. 2.49.

Results

Impact of SLB Composition on Lipid Exchange

Fig. 3.1 shows the mean fluorescence intensity of various composition SLBs after incubation with fluorescently labeled MSP1D1-NLPs and fluorescently labeled control vesicles, normalized by the fluorescence intensity of unlabeled SLBs on glass. Combined with qualitative observations (**Fig. 3.2**), these results provide insight into the influence of target membrane composition and properties for optimizing NLP-SLB interactions and material transfer from NLPs to the SLB. Lipid transfer was markedly enhanced by defects in the supported membrane and prevented in well-packed, gel-phase membranes. The SLB with the most pronounced lipid exchange with NLPs had an outer leaflet composition of DMPC + 5 mol% DOGS-NTA and an inner leaflet composition of DMPC. DMPC membranes are near the phase-transition state at room temperature (T_m = 24 °C). Lipid transfer was further enhanced by doping the SLB mixture with

DOGS-NTA. DOGS-NTA, a nickel-chelating lipid, is capable of specific binding to the polyhistidine-tag of the apolipoprotein, thus acting as an anchor point. When SLBs comprised of DMPC + 5 mol% DOGS-NTA were supported by gel phase inner leaflets comprised of DPPE (T_m = 63 °C), the concentration of defects was reduced[32, 43] and a corresponding reduction in lipid exchange was observed.

In fluid phase membranes comprised of DOPC + 5 mol% DOGS-NTA (T_m = -17 °C), where defects were relatively abundant, lipid exchange was significant and comparable to the amount observed in DMPC + 5 mol% DOGS-NTA. Phase separation in these otherwise homogeneous samples signaled that both DMPC and fluorescent lipid Rhodamine B-DHPE were delivered. In phase separated SLBs comprised of an inner DPPC (T_m = 41 °C) leaflet and an outer DPPE:DOPC (3:7 molar ratio) leaflet, the prevalent fluid phase meant that lipid exchange was only slightly suppressed despite having a gel phase inner leaflet and a fraction of the surface occupied by gel phase domains. Interestingly, incorporation of DOGS-NTA into DPPE:DOPC membranes did not boost lipid exchange the same way it did for DMPC membranes. Instead, incorporation of DOGS-NTA into the phase separated systems reduced the standard deviation across samples, perhaps by driving broader incorporation of fluorescent lipids across the SLB surface as opposed to localized exchange with defects. Homogeneous gel-phase SLBs showed no evidence of lipid exchange upon extended incubation with NLPs.

There was more lipid exchange from NLPs compared to vesicle controls (**Fig. 3.2** insets). When defects were suppressed in DMPC + 5 mol% DOGS-NTA SLBs with inner leaflets comprised of DPPE, similar levels of materials transfer to the SLB were obtained. Fluorescence recovery after photobleaching (FRAP), an indicator of the lateral mobility of fluorescently labeled lipids in the

SLB, was consistently observed in samples incubated with NLPs (see Supporting Information **Fig. 3.S3**). Furthermore, the intensity measurements of SLBs incubated with vesicles were often artificially enhanced by the presence of adsorbed vesicles on the surface (see Supporting Information **Fig. 3.S4**). Taken together, these results demonstrate that NLPs offer an improvement over vesicle incubation and are a viable delivery vehicle for transferring small biomolecules such as lipids to a variety of SLB compositions. Exchange is optimized in the presence of defects or, when defects are suppressed, the presence of specific, NLP binding lipids at the SLB surface.

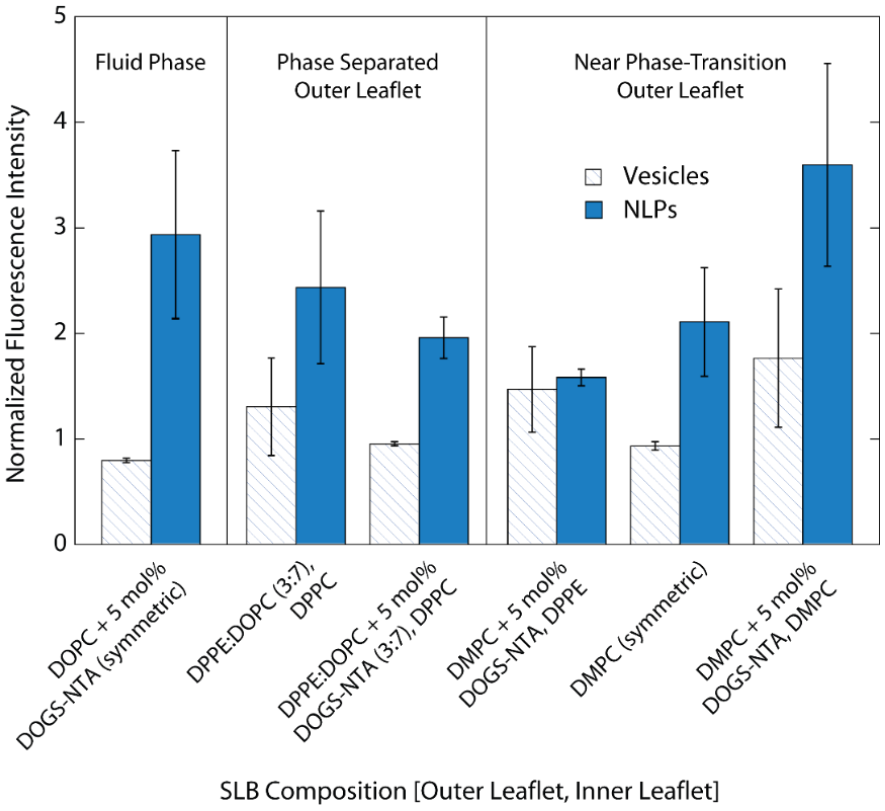

Fig. 3.1. Degree of lipid transfer as a function of composition, as indicated by the mean fluorescence intensity of SLBs after incubation with MSP1D1-NLPs and vesicles containing 2 mol% Rhodamine-DHPE at room temperature, normalized by the fluorescence intensity of unlabeled SLBs on glass. Transfer was enhanced by the presence of bilayer defects, which are abundant in fluid phase (DOPC) membranes and in membranes not coupled to a gel phase (DPPC or DPPE) inner leaflet. For near phase-transition (DMPC) membranes, transfer was further enhanced by addition of DOGS-NTA, a nickel-chelating lipid capable of specific binding to NLPs via the polyhistidine-tag incorporated in each apolipoprotein sequence.

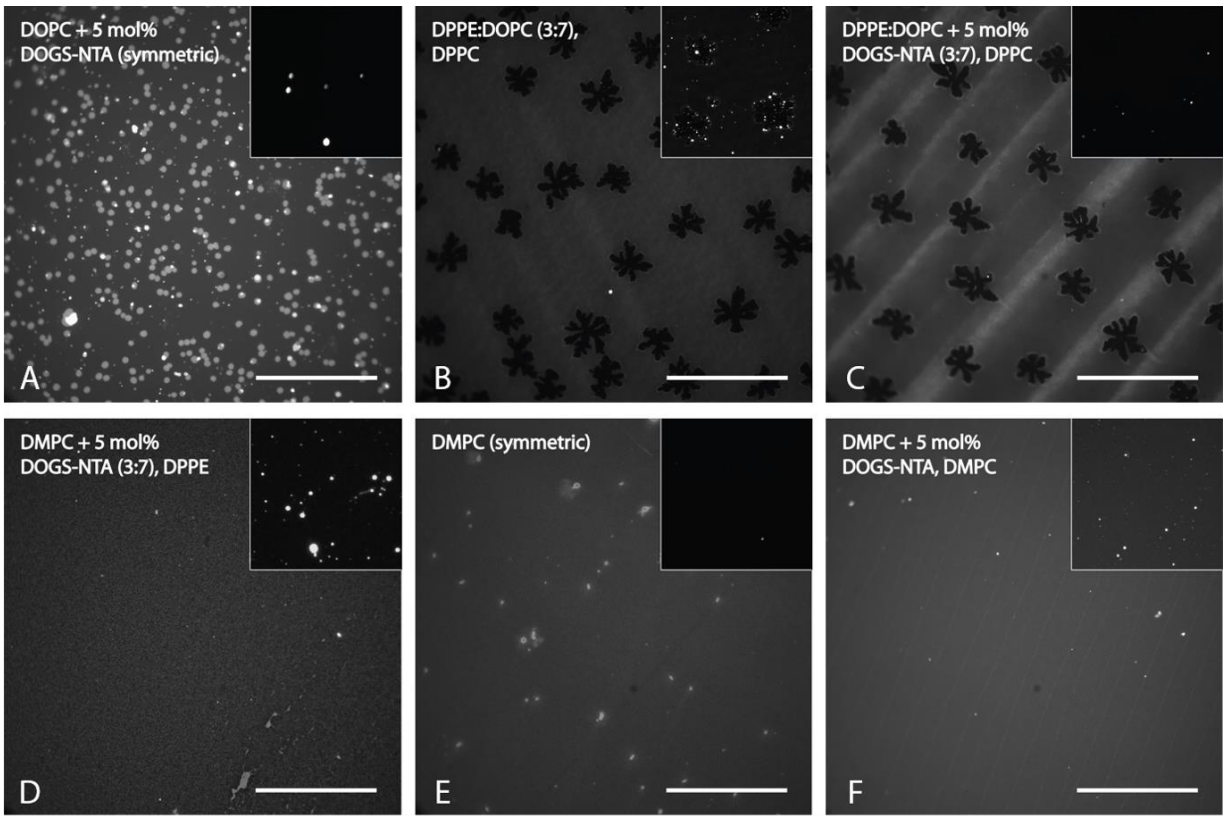

Fig. 3.2. FM images of different composition (label: outer leaflet, inner leaflet) SLBs after incubation with MSP1D1-NLPs and vesicles (insets) containing fluorescent lipid Rhodamine B-DHPE (scale bar = 100 µm for image and inset) at room temperature. (A) Introduction of DMPC from NLPs into fluid phase DOPC SLBs resulted in phase separation and partitioning of the fluorophore into liquid-disordered (L_o) domains. (B, C) In phase-separated DPPE:DOPC SLBs, gel-phase domains appeared dark in contrast with the surrounding fluid-phase matrix. (D) Lipid transfer was suppressed in DMPC SLBs coupled to a gel-phase inner leaflet despite having polyhistidine-binding DOGS-NTA. Exchange in DMPC membranes was enhanced by (E) changing the inner leaflet to DMPC, (F) and then incorporating DOGS-NTA. Intensity was scaled identically for all images shown here.

AFM of SLBs Incubated with NLPs

Topographic images acquired by AFM suggest a highly complex mechanism of interaction between NLPs and SLBs. **Fig. 3.3** shows AFM images of SLBs with outer and inner leaflets comprised of DMPC + 5 mol% DOGS-NTA and DPPE, respectively, incubated with and without NLPs. Phase separation and defects in the form of transmembrane holes (depth ~ 5 nm) are evident in the control sample. This microstructure is typical for DMPC membranes which reside

in near-transition states at room temperature. In the sample incubated with NLPs, there is no discernable phase separation and holes are absent from the surface. There are also ring-like features with an average height of ~1 nm distributed across the surface. In previous attempts to image the interaction between NLPs and the SLB *in situ*, nonspecific adsorption of NLPs to the AFM probe disrupted image acquisition. Consequentially, it was difficult to determine the exact mechanism behind this complex surface rearrangement. However, the size distribution of the rings (122.1 ± 85 nm) was comparable to that of defects in the control sample (143.2 ± 74 nm), suggesting that defects act as docking sites for the NLPs and play a key a role in mediating the formation of the final nanostructure.

Fig. 3.4 shows AFM images of SLBs with outer and inner leaflets comprised of DPPC:DOPC + 5 mol% DOGS-NTA:Chol (9:9:2 molar ratio) and DPPE, respectively, incubated with and without NLPs. Phase separation and transmembrane holes were again observed in the control sample. Like the DMPC membrane results, incubating NLPs with DPPC:DOPC:Chol membranes appeared to result in suppressed phase separation. Line profile scans exposed defects with a similar size distribution (501.2 ± 334 nm) to that of defects observed in the control sample (456.7 ± 234 nm). However, defects in SLBs incubated with NLPs had a shortened depth of ~1.5 nm compared to ~5 nm in the control samples. Assuming that lipid transfer from the NLPs resulted in filling of defects in both of the compositions examined using AFM, increased lateral pressure from lipid crowding could have induced mixing in the system and suppressed phase separation as observed.[39]

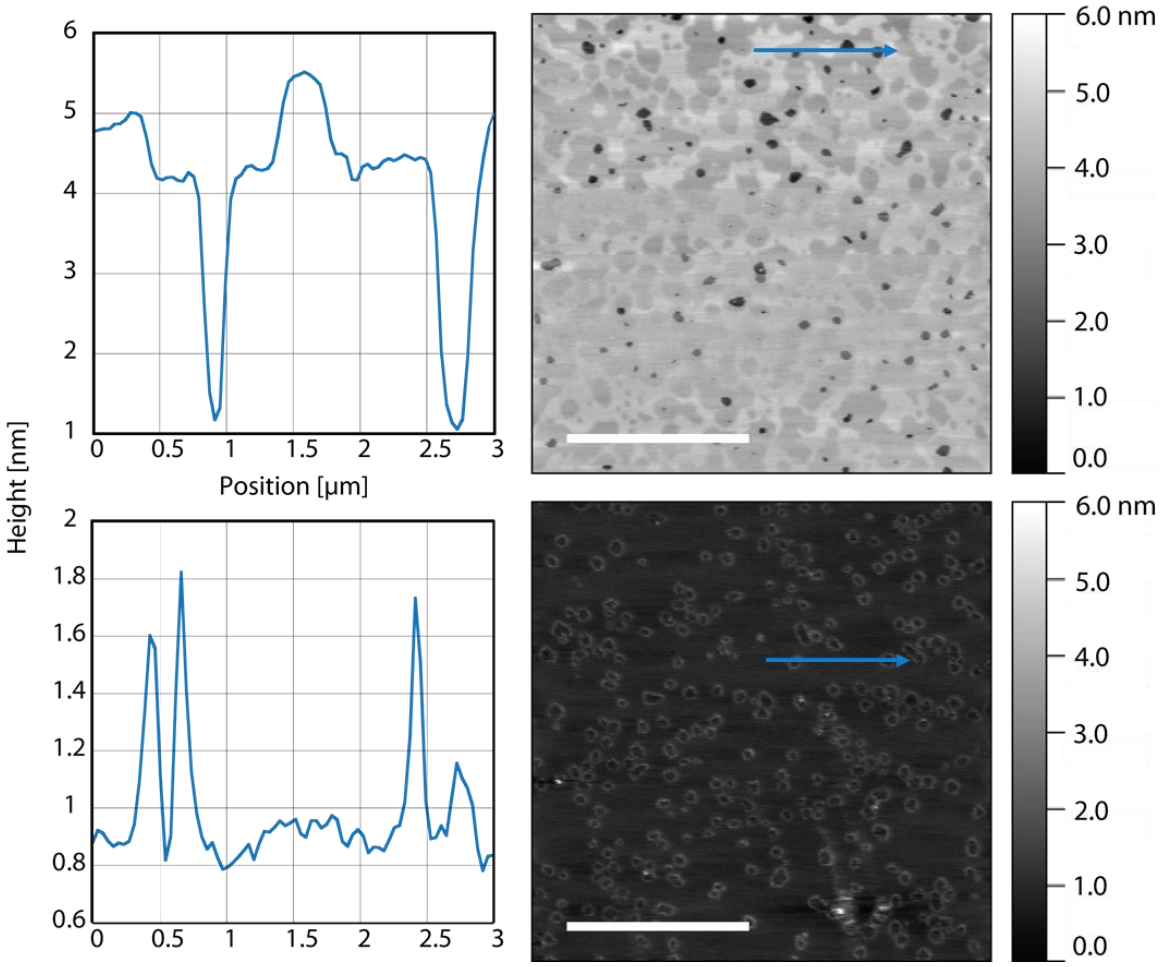

Fig. 3.3. (Right) AFM topographic images (scale bar = 3 µm) and (Left) line profile scans of DMPC + 5 mol% DOGS-NTA (inner leaflet DPPE) SLBs recorded at room temperature in PBS buffer, after 12 hr incubation and subsequent rinsing. (Top) SLBs incubated without NLPs exhibited defects in the form of holes with an average depth of ~ 5 nm due to solubilization of lipid over time. Since SLBs were imaged under ambient conditions near the phase transition temperature of DMPC (T_m = 24 ˚C), phase separation was observed. (Bottom) SLBs incubated with NLPs presented raised ring-like features. Line profile scans revealed that holes were not present, suggesting that defects had become filled as a result of materials transfer from NLPs.

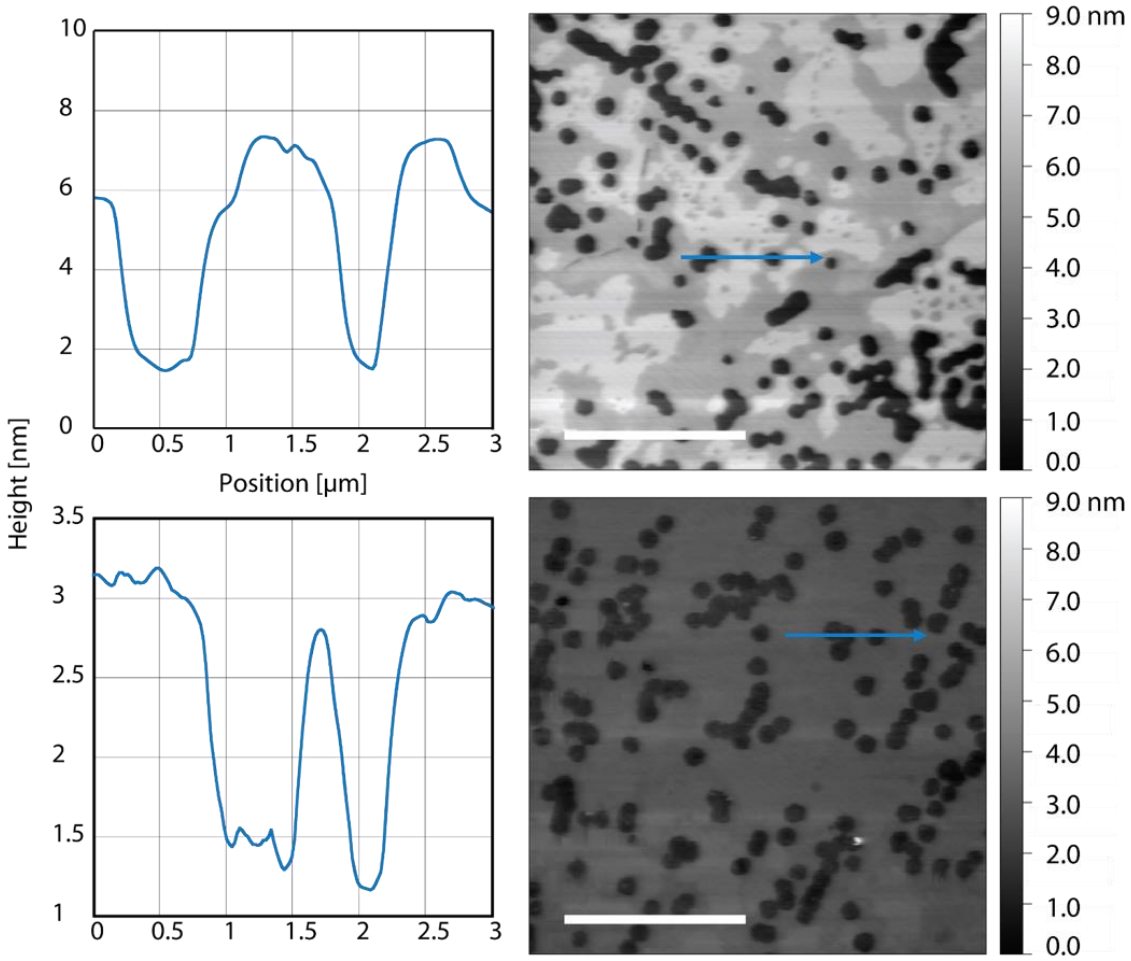

Fig. 3.4. (Right) AFM topographic images (scale bar = 3 µm) and (Left) line profile scans of DPPC:DOPC + 5 mol% DOGS-NTA:Chol (9:9:2) (inner leaflet DPPC) SLBs recorded at room temperature in PBS buffer, after 12 hr incubation and subsequent rinsing. (Top) SLBs incubated without NLPs exhibited phase separation and defects in the form of holes with an average depth of ~5 nm. (Bottom) Phase separation was suppressed in SLBs incubated with NLPs. Further, defects appeared partially filled with an average depth of ~1.5 nm.

Lipid Transfer between NLPs and PAA-Cushioned SLBs

Fig. 3.5A shows FM images of a patterned PAA-cushioned membrane labeled with OG-DHPE. As seen in **Fig. 3.5B**, addition of Δ49ApoA1-NLPs containing TR-DHPE resulted in lipid transfer, made apparent by co-localization of TR-DHPE and OG-DHPE emission on membrane patches. When the experiment was repeated with CLIP-ErbB2-NLPs (labeled with CLIP-Cell TMR-Star), the SLB was not labeled to reduce background noise. After a 12 hr incubation period, CLIP-

ErbB2/HER2 transfer was confirmed when emission from the conjugated fluorescent substrate, CLIP-Cell TMR-Cell was detected in the SLB. Details on negative control trials are described in Supporting Information. FRAP experiments revealed that CLIP-ErbB2/HER2 exhibited lateral mobility, but only in areas where the membrane appeared to be suspended between PAA patches (**Fig. 3.6**). Restricted mobility in directly supported membranes was likely due to the pH-sensitive properties of PAA cushions. When stored in acidic conditions (pH < 4) or in solutions with low ionic strength, the polymer assumes a collapsed structure where lateral diffusivity in the supported bilayer can be reduced by several orders of magnitude compared to a fluid bilayer supported on an oxide substrate.[34] While not done in this experiment, it is possible to induce mobility in PAA-cushioned SLBs by adjusting the pH to 7.4 or higher. Under neutral to alkaline conditions, coupling between the cushion and the lipid bilayer becomes weakened as ionization of PAA chains causes the former to swell with water.[34] Note that effective pH equilibration requires that ions be able to diffuse into the water layer between the membrane and underlying substrate. However, a tightly packed, continuous bilayer may effectively "seal" the PAA cushion from the bulk solution. This issue could be circumvented by introducing defects or channels into the membrane. Straightforward methods for doing so include, patterning, thermal cycling, and incorporation of transmembrane channel proteins such as gramicidin. In general, pH-sensitive membranes such as PAA-cushioned SLBs offer a convenient mode of controlling the diffusivity of proteins in model systems.

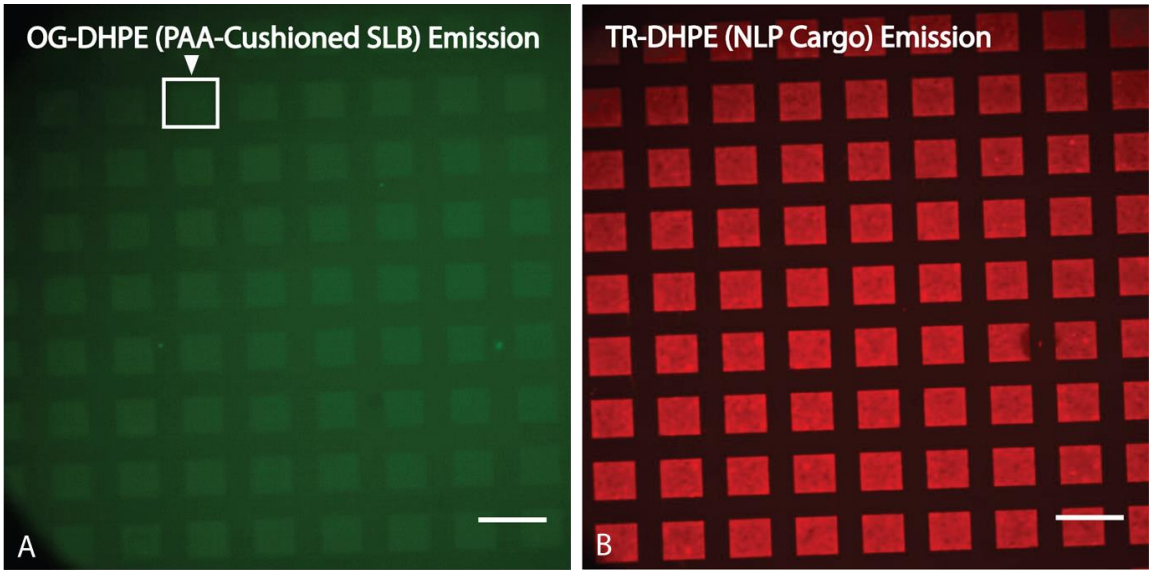

Fig. 3.5. FM of an OG-DHPE-labeled micropatterned PAA-cushioned (DMPC + 5 mol% DOGS-NTA) SLB after incubation with NLPs containing TR-DHPE (scale bar = 200 µm). Lipid transfer was evidenced by the co-localization of fluorescent emission from (A) OG-DHPE and (B) TR-DHPE.

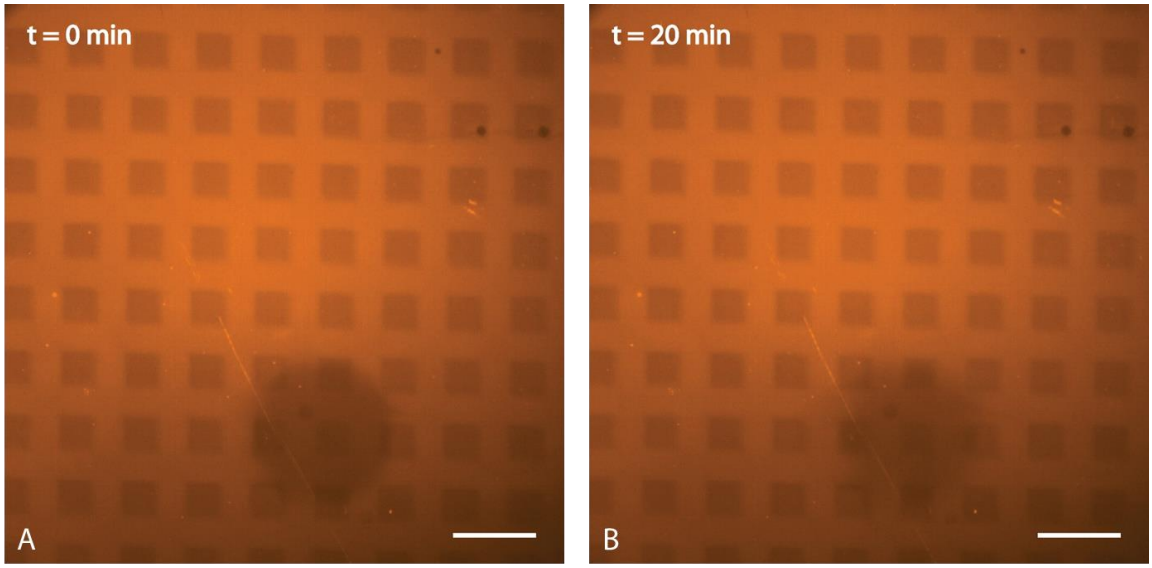

Fig. 3.6. FRAP of a micropatterned PAA-cushioned (DMPC + 5 mol% DOGS-NTA) SLB after incubation with CLIP-ErbB2-NLPs (scale bar = 200 µm). Because the bilayer was deposited after patterning and passivation of exposed surfaces, parts of the membrane "bridged" across PAA patches (squares) to form a continuous bilayer across the surface. (A) Photobleaching a small region of the SLB (darkened circular area, diameter ~150 µm) verified that CLIP-ErbB2/HER2 incorporated into both directly supported and suspended areas of the bilayer. (B) Partial recovery during FRAP, evidenced by brightening and the blurring of edges in the photobleached region, was observed in suspended regions over time.

Mechanisms of Transfer

Enhanced transfer in samples with more defects and containing DOGS-NTA suggests that materials delivery from NLPs can be regulated by the target lipid environment and by the presence of apolipoprotein-binding molecules. These results are in accord with previous studies on lipid exchange between NLPs and other biomimetic lipid systems.[38-39] Still, the vast parameter space around this complex interaction makes it difficult to define an exact mechanism. Given the scarcity of information pertaining to NLP-SLB systems, tangential research from HDL particles may provide clues on the range of behaviors that might be further explored. In biological systems, HDL particles are thought to deliver lipids directly to cell membranes upon binding with the scavenger receptor, class B type 1 (SR-B1).[44-45] Importantly, lipid uptake is selective and does not compromise the structural fidelity of the HDL particle when mediated by SR-B1.[11] Yet in another independent study on model membranes, HDL particles appear to integrate upon contact even in the absence of surface receptors.[8] Further, associated apolipoproteins do not appear to discriminate between different types of lipid domains.[46] Unsurprisingly, NLPs exhibit similar capacity for cargo delivery through either specific or non-specific interactions with SLBs. In the case of the latter, defects appear to serve as the principle sites for materials exchange based on the results of this study. Continuing efforts to determine mechanisms of NLP-SLB interactions would benefit from examining the kinetics of lipid transfer and the residence time of apolipoprotein at the SLB surface, with and without specific binding receptor analogs.

Conclusions

This work explored the viability of using NLPs to deliver lipids and proteins to SLBs. FM experiments revealed that the efficacy of lipid exchange depended on the composition of the

target bilayer. Transfer was improved by incorporating polyhistidine tag-binding lipids into the SLB which selectively bound NLP apolipoproteins encoded with polyhistidine tags. The most dominant influence on the magnitude of lipid exchange appeared to be the concentration of defects in the SLB. AFM experiments showed that incubation with NLPs resulted in the formation of topographical features with similar size distribution as that of defects observed in control samples. Although the structural rearrangement was too complex to outline a clear mechanism, it verified interactions between NLPs and the SLB, which resulted in changes to the structure of the SLB as well as direct transfer of cargo from the NLP to the SLB. Lastly, preliminary FM experiments with NLPs containing embedded receptor tyrosine kinase CLIP-ErbB2/HER2 demonstrated that protein cargoes could be delivered from NLPs to PAA-cushioned SLBs.

There are notable advantages in using model membrane systems - NLPs enable access to a growing selection of membrane proteins, while SLBs create opportunities to study them in modular, two-dimensional environments. Indeed, the integration of cell-free expression into NLPs is a growing area of focus and eliminates challenging purification steps of traditional cell-based protein expression. The SLB platform is also very flexible. The composition of the SLB can also be readily adjusted to enhance or decrease loading to suit specific applications, as well as investigate the impact of membrane composition on protein function in a controlled fashion. Nevertheless, there are limitations to this approach. Namely, aging effects necessitate that experiments be conducted within a short period of time. NLPs should be utilized within 1 week of synthesis, as DLS experiments revealed that they are prone to aggregation over time (unpublished data). Likewise, SLBs are susceptible to long term lipid solubilization and should be utilized within 24 hr or kept in lipid-saturated solution conditions to prevent equilibration

induced desorption. Solution conditions must also be considered carefully. While we did not closely examine NLP stability under varied ionic strength conditions, we found that NLPs tended to aggregate in deionized water and therefore recommend that they be stored in solutions with sufficiently high ionic strength (> 100 mM). In general, NLP aggregates can be dispersed by quick sonication, vortexing, or rapid pipetting.

In conclusion, this work shows that NLP-mediated transfer can be used to introduce lipids and membrane proteins into SLBs under well-defined conditions. Next steps should focus on transfer of different membrane proteins to SLBs, with special attention paid to target membrane composition to maximize loading. Equally important will be verification of the structural fidelity and functionality of ErbB2/HER2 after delivery, likely through observation of domain recognition and binding by fluorescently labeled antibodies.

Associated Content

Detailed methods, sample specifications, and additional figures in **Supporting Information**.

Author Information

Corresponding Author

*E-mail: tlkuhl@ucdavis.edu.

Author Contributions

The manuscript was written through contributions of all authors. All authors have given approval to the final version of the manuscript.

Funding Sources

This work was supported by the National Science Foundation Chemistry Division through grant CHE-1413745, the University of California, Davis Biotechnology Training Program Fellowship, and

the National Institutes of Health under award numbers R21AI120925, R01CA155642 and R01GM117342. Work was also performed under the auspices of the U.S. Department of Energy by Lawrence Livermore National Laboratory under Contract DE-AC52-07NA27344.

Acknowledgement

AFM images were recorded at the NEAT ORU Keck Spectral Instrument Facility. We thank Prof. Marjorie Longo and Prof. Tina Jeoh at the University of California, Davis for providing access to the instruments used to characterize NLPs.

References

1. Jonas, A.; Kezdy, K. E.; Wald, J. H., Defined apolipoprotein A-I conformations in reconstituted high density lipoprotein discs. *The Journal of biological chemistry* **1989,** *264* (9), 4818-24.
2. Fischer, N. O.; Weilhammer, D. R.; Dunkle, A.; Thomas, C.; Hwang, M.; Corzett, M.; Lychak, C.; Mayer, W.; Urbin, S.; Collette, N.; Chiun Chang, J.; Loots, G. G.; Rasley, A.; Blanchette, C. D., Evaluation of Nanolipoprotein Particles (NLPs) as an In Vivo Delivery Platform. *PLoS ONE* **2014,** *9* (3), e93342.
3. Numata, M.; Grinkova, Y. V.; Mitchell, J. R.; Chu, H. W.; Sligar, S. G.; Voelker, D. R., Nanodiscs as a therapeutic delivery agent: inhibition of respiratory syncytial virus infection in the lung. *International journal of nanomedicine* **2013,** *8*, 1417-1427.
4. Cappuccio, J. A.; Blanchette, C. D.; Sulchek, T. A.; Arroyo, E. S.; Kralj, J. M.; Hinz, A. K.; Kuhn, E. A.; Chromy, B. A.; Segelke, B. W.; Rothschild, K. J.; Fletcher, J. E.; Katzen, F.; Peterson, T. C.; Kudlicki, W. A.; Bench, G.; Hoeprich, P. D.; Coleman, M. A., Cell-free co-expression of functional membrane proteins and apolipoprotein, forming soluble nanolipoprotein particles. *Molecular & cellular proteomics : MCP* **2008,** *7* (11), 2246-53.
5. He, W.; Scharadin, T. M.; Saldana, M.; Gellner, C.; Hoang-Phou, S.; Takanishi, C.; Hura, G. L.; Tainer, J. A.; Carraway Iii, K. L.; Henderson, P. T.; Coleman, M. A., Cell-free expression of functional receptor tyrosine kinases. *Scientific Reports* **2015,** *5*, 12896.
6. Leitz, A. J.; Bayburt, T. H.; Barnakov, A. N.; Springer, B. A.; Sligar, S. G., Functional reconstitution of beta(2)-adrenergic receptors utilizing self-assembling Nanodisc technology. *Biotechniques* **2006,** *40* (5), 601-+.
7. Gilmore, S. F.; Blanchette, C. D.; Scharadin, T. M.; Hura, G. L.; Rasley, A.; Corzett, M.; Pan, C.-x.; Fischer, N. O.; Henderson, P. T., Lipid Cross-Linking of Nanolipoprotein Particles Substantially Enhances Serum Stability and Cellular Uptake. *ACS applied materials & interfaces* **2016,** *8* (32), 20549-20557.
8. Plochberger, B.; Röhrl, C.; Preiner, J.; Rankl, C.; Brameshuber, M.; Madl, J.; Bittman, R.; Ros, R.; Sezgin, E.; Eggeling, C.; Hinterdorfer, P.; Stangl, H.; Schütz, G. J., HDL particles incorporate into lipid

bilayers – a combined AFM and single molecule fluorescence microscopy study. *Scientific Reports* **2017,** *7* (1), 15886.

9. Rothblat, G. H.; Phillips, M. C., High-density lipoprotein heterogeneity and function in reverse cholesterol transport. *Curr Opin Lipidol* **2010,** *21*.
10. Lund-Katz, S.; Phillips, M. C., High density lipoprotein structure-function and role in reverse cholesterol transport. *Sub-cellular biochemistry* **2010,** *51*, 183-227.
11. Williams, D. L.; de la Llera-Moya, M.; Thuahnai, S. T.; Lund-Katz, S.; Connelly, M. A.; Azhar, S.; Anantharamaiah, G. M.; Phillips, M. C., Binding and Cross-linking Studies Show That Scavenger Receptor BI Interacts with Multiple Sites in Apolipoprotein A-I and Identify the Class A Amphipathic α-Helix as a Recognition Motif. *Journal of Biological Chemistry* **2000,** *275* (25), 18897-18904.
12. Rothblat, G. H.; Phillips, M. C., High-density lipoprotein heterogeneity and function in reverse cholesterol transport. *Current opinion in lipidology* **2010,** *21* (3), 229-238.
13. Chromy, B. A.; Arroyo, E.; Blanchette, C. D.; Bench, G.; Benner, H.; Cappuccio, J. A.; Coleman, M. A.; Henderson, P. T.; Hinz, A. K.; Kuhn, E. A.; Pesavento, J. B.; Segelke, B. W.; Sulchek, T. A.; Tarasow, T.; Walsworth, V. L.; Hoeprich, P. D., Different apolipoproteins impact nanolipoprotein particle formation. *J Am Chem Soc* **2007,** *129* (46), 14348-54.
14. Cleveland, T. E.; He, W.; Evans, A. C.; Fischer, N. O.; Lau, E. Y.; Coleman, M. A.; Butler, P., Small-angle X-ray and neutron scattering demonstrates that cell-free expression produces properly formed disc-shaped nanolipoprotein particles. *Protein Science* **2018,** *27* (3), 780-789.
15. Blanchette, C. D.; Cappuccio, J. A.; Kuhn, E. A.; Segelke, B. W.; Benner, W. H.; Chromy, B. A.; Coleman, M. A.; Bench, G.; Hoeprich, P. D.; Sulchek, T. A., Atomic force microscopy differentiates discrete size distributions between membrane protein containing and empty nanolipoprotein particles. *Biochimica Et Biophysica Acta-Biomembranes* **2009,** *1788* (3), 724-731.
16. Bayburt, T. H.; Grinkova, Y. V.; Sligar, S. G., Self-Assembly of Discoidal Phospholipid Bilayer Nanoparticles with Membrane Scaffold Proteins. *Nano Letters* **2002,** *2* (8), 853-856.
17. Bricarello, D. A.; Smilowitz, J. T.; Zivkovic, A. M.; German, J. B.; Parikh, A. N., Reconstituted lipoprotein: a versatile class of biologically-inspired nanostructures. *ACS Nano* **2011,** *5* (1), 42-57.
18. Gao, T. J.; Petrlova, J.; He, W.; Huser, T.; Kudlick, W.; Voss, J.; Coleman, M. A., Characterization of De Novo Synthesized GPCRs Supported in Nanolipoprotein Discs. *Plos One* **2012,** *7* (9).
19. Rawson, S.; Davies, S.; Lippiat, J. D.; Muench, S. P., The changing landscape of membrane protein structural biology through developments in electron microscopy. *Molecular membrane biology* **2016,** *33* (1-2), 12-22.
20. Yin, H.; Flynn, A. D., Drugging Membrane Protein Interactions. *Annual review of biomedical engineering* **2016,** *18* (1), 51-76.
21. White, S. Membrane Proteins of Known 3D Structure. http://blanco.biomol.uci.edu/mpstruc/ (accessed 21 January).
22. Ghosh, E.; Kumari, P.; Jaiman, D.; Shukla, A. K., Methodological advances: the unsung heroes of the GPCR structural revolution. *Nature Reviews Molecular Cell Biology* **2015,** *16*, 69.
23. Dawaliby, R.; Trubbia, C.; Delporte, C.; Masureel, M.; Van Antwerpen, P.; Kobilka, B. K.; Govaerts, C., Allosteric regulation of G protein–coupled receptor activity by phospholipids. *Nature Chemical Biology* **2015,** *12*, 35.

24. Saliba, A.-E.; Vonkova, I.; Gavin, A.-C., The systematic analysis of protein–lipid interactions comes of age. *Nature Reviews Molecular Cell Biology* **2015,** *16*, 753.
25. Scharadin, T. M.; Saldana, M.; Schlein, M.; Hoang-Phou, S.; Trans, D.; Chang, D.; He, W.; Lam, K.; Carraway, K. L.; Coleman, M. A.; Henderson, P. T., Using NLPs to study EGFR structure, activation, and inhibition. *Cancer Research* **2014,** *74* (19).
26. Scharadin, T. M.; He, W.; Yiannakou, Y.; Tomilov, A. A.; Saldana, M.; Cortopassi, G. A.; Carraway, K. L., 3rd; Coleman, M. A.; Henderson, P. T., Synthesis and biochemical characterization of EGF receptor in a water-soluble membrane model system. *PloS one* **2017,** *12* (6), e0177761-e0177761.
27. Lai, G.; Renthal, R., Integral Membrane Protein Fragment Recombination after Transfer from Nanolipoprotein Particles to Bicelles. *Biochemistry* **2013,** *52* (52), 9405-9412.
28. Gao, T. J.; Blanchette, C. D.; He, W.; Bourguet, F.; Ly, S.; Katzen, F.; Kudlicki, W. A.; Henderson, P. T.; Laurence, T. A.; Huser, T.; Coleman, M. A., Characterizing diffusion dynamics of a membrane protein associated with nanolipoproteins using fluorescence correlation spectroscopy. *Protein Science* **2011,** *20* (2), 437-447.
29. Watkins, E. B.; Kuhl, T. L.; Majewski, J.; Miller, C. E.; Johannes, L.; Gao, H.; Dennison, A. J., Glycolipid clustering and lipid reorganization induced by bacterial toxin binding to model membranes. *European Biophysics Journal with Biophysics Letters* **2013,** *42*, S157-S157.
30. Li, E.; Merzlyakov, M.; Lin, J.; Searson, P.; Hristova, K., Utility of surface-supported bilayers in studies of transmembrane helix dimerization. *Journal of Structural Biology* **2009,** *168* (1), 53-60.
31. Sezgin, E.; Schwille, P., Model membrane platforms to study protein-membrane interactions. *Molecular membrane biology* **2012,** *29* (5), 144-54.
32. Kurniawan, J.; Ventrici de Souza, J. F.; Dang, A. T.; Liu, G.-y.; Kuhl, T. L., Preparation and Characterization of Solid-Supported Lipid Bilayers Formed by Langmuir–Blodgett Deposition: A Tutorial. *Langmuir* **2018,** *34* (51), 15622-15639.
33. Sezgin, E.; Levental, I.; Mayor, S.; Eggeling, C., The mystery of membrane organization: composition, regulation and roles of lipid rafts. *Nature Reviews Molecular Cell Biology* **2017,** *18*, 361.
34. El-khouri, R. J.; Bricarello, D. A.; Watkins, E. B.; Kim, C. Y.; Miller, C. E.; Patten, T. E.; Parikh, A. N.; Kuhl, T. L., pH Responsive Polymer Cushions for Probing Membrane Environment Interactions. *Nano Letters* **2011,** *11* (5), 2169-2172.
35. Watkins, E.; El-khouri, R. J.; Miller, C.; Seaby, B. G.; Majewski, J.; Marques, C. M.; Kuhl, T., Structure and thermodynamics of lipid bilayers on polyethylene glycol cushions: Fact and fiction of PEG cushioned membranes. *Langmuir* **2011**.
36. Pace, H.; Simonsson Nyström, L.; Gunnarsson, A.; Eck, E.; Monson, C.; Geschwindner, S.; Snijder, A.; Höök, F., Preserved Transmembrane Protein Mobility in Polymer-Supported Lipid Bilayers Derived from Cell Membranes. *Analytical chemistry* **2015,** *87* (18), 9194-9203.
37. Nair, P. M.; Salaita, K.; Petit, R. S.; Groves, J. T., Using patterned supported lipid membranes to investigate the role of receptor organization in intercellular signaling. *Nat. Protoc.* **2011,** *6*, 523.
38. Lai, G.; Forti, K. M.; Renthal, R., Kinetics of lipid mixing between bicelles and nanolipoprotein particles. *Biophysical chemistry* **2015,** *197*, 47-52.
39. Zeno, W. F.; Rystov, A.; Sasaki, D. Y.; Rishud, S. H.; Longo, M. L., Crowding-Induced Mixing Behavior of Lipid Bilayers: Examination of Mixing Energy, Phase, Packing Geometry, and Reversibility.

Langmuir **2016,** *32* (18), 4688-4697.

40. Patriarchi, T.; Shen, A.; He, W.; Baikoghli, M.; Cheng, R. H.; Xiang, Y. K.; Coleman, M. A.; Tian, L., Nanodelivery of a functional membrane receptor to manipulate cellular phenotype. *Scientific Reports* **2018,** *8* (1), 3556.
41. Kurniawan, J.; Kuhl, T. L., Characterization of solid-supported dipalmitoylphosphatidylcholine membranes containing cholesterol. *Langmuir* **2015,** *31* (8), 2527-32.
42. Zeno, W. F.; Hilt, S.; Aravagiri, K. K.; Risbud, S. H.; Voss, J. C.; Parikh, A. N.; Longo, M. L., Analysis of lipid phase behavior and protein conformational changes in nanolipoprotein particles upon entrapment in sol-gel-derived silica. *Langmuir* **2014,** *30* (32), 9780-8.
43. Kienle, D. F.; de Souza, J. V.; Watkins, E. B.; Kuhl, T. L., Thickness and refractive index of DPPC and DPPE monolayers by multiple-beam interferometry. *Analytical and bioanalytical chemistry* **2014,** *406* (19), 4725-33.
44. Shen, W.-J.; Azhar, S.; Kraemer, F. B., SR-B1: A Unique Multifunctional Receptor for Cholesterol Influx and Efflux. *Annual review of physiology* **2018,** *80*, 95-116.
45. Plochberger, B.; Axmann, M.; Röhrl, C.; Weghuber, J.; Brameshuber, M.; Rossboth, B. K.; Mayr, S.; Ros, R.; Bittman, R.; Stangl, H.; Schütz, G. J., Direct observation of cargo transfer from HDL particles to the plasma membrane. *Atherosclerosis* **2018,** *277*, 53-59.
46. Arnulphi, C.; Sánchez, S. A.; Tricerri, M. A.; Gratton, E.; Jonas, A., Interaction of human apolipoprotein A-I with model membranes exhibiting lipid domains. *Biophysical journal* **2005,** *89* (1), 285-295.

Supporting Information

PAA Cushion Preparation (Detailed Protocol)

PAA cushions were prepared using spin-coating methods described by El-Khouri et al.[1] PAA (450k MW, 0.1% cross-linked, Sigma-Aldrich, Inc.) was dissolved in methanol (≥ 99% purity, Sigma-Aldrich**)** at a concentration of 1 mg/mL, stirred overnight (<16 hr), and subsequently passed through a 0.2 µM Whatman PFTE filter. Next, coverslips were functionalized with aminopropyltriethoxysilane (APTES) by immersion in a gently stirred solution of ~1 mM APTES (Gelest Inc.) in toluene (≥ 99% purity, Sigma-Aldrich) for one 1 hr. Silanized samples were then rinsed with toluene, dried under a light stream of nitrogen (specialty grade, 99.998% pure), and cured for 2 hr at 100 °C.

Once samples had cooled to room temperature, PAA was deposited by gently injecting dissolved PAA on the silanized surface and spin-coating for 2 min at 2000 RPM. Covalent linkage between the PAA and APTES was promoted through subsequent curing for 2 hr at 200 °C. Finally, PAA substrates were immersed in Tris buffer (pH 9) to convert anhydrides to carboxylates and relieve mechanical stresses in the polymer layer. Areas exposed during photolithography were subsequently treated with AquaSil siliconizing fluid (Thermo Fisher Scientific) per manufacturer instructions to render them resistant to nonspecific protein adsorption.

MSP1D1-NLP Assembly (Detailed Protocol)

NLPs stabilized with membrane scaffold protein MSP1D1 (MSP1D1-NLPs) were assembled using methods adopted from protocols described by Zeno et al.[2] A stoichiometric excess (4.3 mg) of DMPC containing 2 mol% Rhodamine-DHPE was dried in a glass vial with nitrogen (specialty grade, 99.998% pure) and placed under mild vacuum for at least 6 hr. The lipid mixture was then rehydrated in reconstitution buffer consisting of 17 mg of sodium cholate hydrate added to 1 mL of Tris buffer (pH 7.4), transferred to a plastic centrifuge tube, mixed using a vortex shaker at room temperature for 30 min, and then sonicated for 10 min.

2 mg of lyophilized apolipoprotein MSP1D1 (Cube Biotech, Inc.), resuspended in 0.5 mL of MilliQ deionized water, was then added to the lipid mixture such that the molar ratio of lipid-protein was 80:1. The lipid-protein mixture was subsequently incubated for 2 hr, alternating between light shaking at 4 °C and 37 °C every 20 min. After incubation, the mixture was transferred to a 10 kDa MWCO Slide-A-Lyzer dialysis cassette (Thermo Fisher Scientific) and dialyzed at 4 °C, in Tris buffer (pH 7.4) at over 300 times the sample volume (4 buffer exchanges over 48 hr) to promote cholate removal and NLP assembly. NLPs were isolated from the dialyzed mixture by nickel affinity purification.

Table 3.S1. Supported Lipid Bilayer Sample Details

Imaging Method	Outer Leaflet	Inner Leaflet	Support	Preparation Method
FM	DOPC+ 5 mol% DOGS-NTA	DOPC+ 5 mol% DOGS-NTA	Glass Coverslip	Vesicle Fusion
FM	DPPE:DOPC (3:7)	DPPC	Glass Coverslip	LB-LB
FM	DPPE:DOPC + 5 mol% DOGS-NTA (3:7)	DPPC	Glass Coverslip	LB-LB
FM	DMPC + 5 mol% DOGS-NTA	DPPE	Glass Coverslip	LB-LB
FM	DMPC	DMPC	Glass Coverslip	LB-LB
FM	DMPC + 5 mol% DOGS-NTA	DMPC	Glass Coverslip	LB-LB
AFM	DMPC + 5 mol% DOGS-NTA	DPPE	Mica	LB-LB
AFM	DPPC:DOPC + 5 mol% DOGS-NTA:Chol (9:9:2)	DPPE	Mica	LB-LB
FM	DMPC + 5 mol% DOGS-NTA	DMPC + 5 mol% DOGS-NTA	PAA-Cushion	LB-LS

SDS-PAGE

SDS-PAGE on Δ49ApoA1-NLPs (**Fig. 3.S1A**) and CLIP-ErbB2-NLPs (**Fig. 3.S1B**) was performed using NuPAGE Novex™ 4-12% Bis-Tris protein gels (Thermo Fisher Scientific). Samples were heated to 98 °C for 5 min with NuPAGE LDS Sample Buffer and NuPAGE reducing Agent, mixed per manufacturer specifications. Gels were run at 200V for approximately 30 min. Bands were compared against NuPAGE Novex™ pre-stained standard to determine molecular weight.

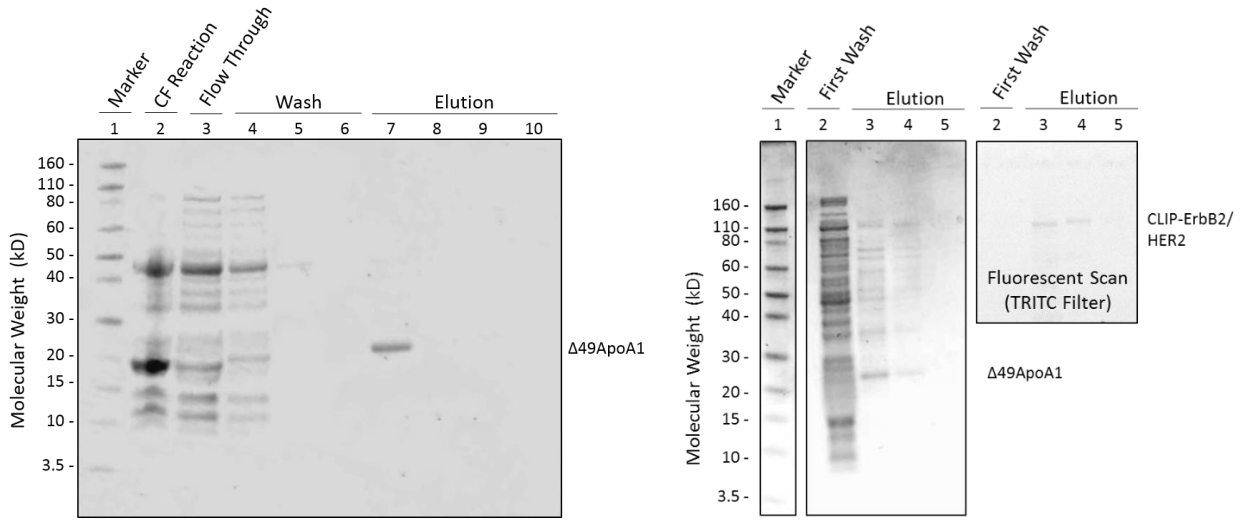

Fig. 3.S1. SDS-PAGE gels of (A) Δ49ApoA1-NLPs and (B) CLIP-ErbB2-NLPs. The sizes of CLIP-ErbB2/HER2 and Δ49ApoA1 (lacking post-translational modification) are ~120 kDa and ~26 kDa, respectively.

SDS-PAGE on MSP1D1-NLPs (**Fig. 3.S2**) was performed using Mini-PROTEAN® TGX Precast Gels (Bio-Rad Laboratories, Inc.). Samples were heated to 80 °C for 10 min with Laemmli sample buffer and 1-mercaptoethanol, mixed per manufacturer specifications. Gels were run at 200V for approximately 30 min. Bands were compared against Precision Plus Protein™ pre-stained standard to determine molecular weight.

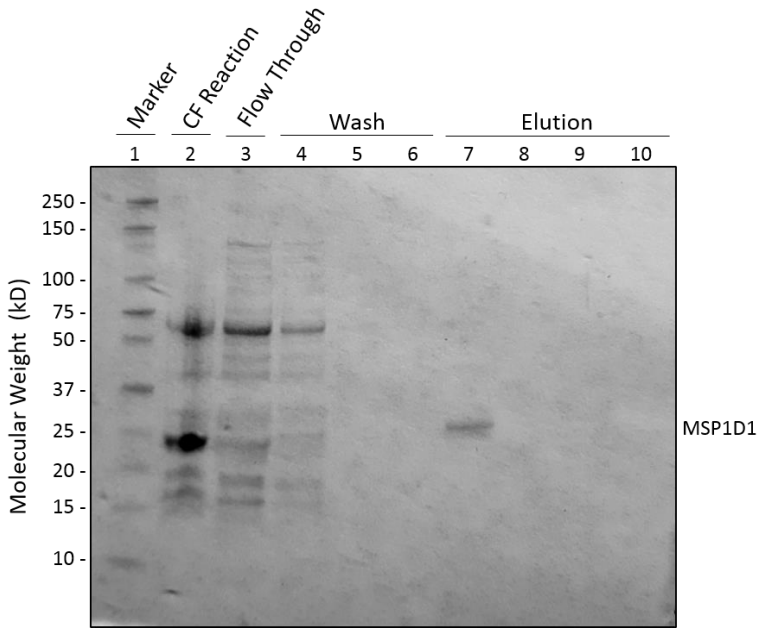

Fig. 3.S2. SDS-PAGE gel of MSP1D1-NLPs. The size of MSP1D1 is ~25 kDa.

UV-Vis Spectrophotometry

Protein concentration was quantified by measuring peak absorbance at 280 nm and applying the Beer-Lambert Law (Eqn. S1) where *A* is the measured absorbance, ε is the protein's intrinsic extinction coefficient, *b* is the path length (1 cm in this case), and *c* is the concentration.

$$A = \varepsilon * b * c \qquad \textbf{Eqn. S1}$$

The absorbance spectrum of a control solution with a known concentration of vesicles composed of DMPC containing 2 mol% Rhodamine-DHPE was recorded and used to calibrate for vesicle contributions to the spectra obtained for NLPs.

Particle Size Analysis of NLPs

The Stokes diameter, d_s reported using dynamic light scattering assumes a spherical particle. This value can be used to derive a discoidal diameter, d_D using the following equation Eqn. S2, which equates the area of a sphere to that of a cylinder.[3] The height of the disc, *h* is assumed to be 5 nm, the height of a typical bilayer in an NLP.

$$d_D = \left(\frac{2d_s^3}{3h}\right)^{1/2} \qquad \textbf{Eqn. S2}$$

Excluding large contaminants (> 1000 nm diameter), the size distribution measurements of MSP1D1-NLP mixtures, measured in terms of the Stokes diameter were bimodal. One peak, centered at 203.1 ± 57.0 nm, was attributed to residual vesicles in solution. The other, centered at 14.8 ± 2.7 nm, was ascribed to NLPs and corresponded to a discoidal diameter of 20.7 ± 1.6 nm.

Negative Control – CLIP-Cell TMR-Star

A negative control experiment was conducted to determine whether fluorescent substrate CLIP-Cell TMR-Star inserted into the hydrophobic domain of the NLP bilayer. Negative control NLPs were expressed using cell-free expression and subjected to the same CLIP-Cell TMR-Star conjugation protocol that was used to label CLIP-ErbB2-NLPs before purification. When these NLPs were incubated with unlabeled SLBs, no detectable fluorescence was imparting into the sample. This indicated CLIP-Cell TMR-Star did not insert into NLPs in the absence of a CLIP-tagged membrane protein and that the purification scheme was sufficient for removing unconjugated substrate from the final product.

Fluorescence Intensity Analysis

Mean fluorescence intensity was measured as the grayscale intensity (arbitrary unit) averaged across 10+ raw images recorded from across the surface of each sample. Illumination conditions and temperature (T = 25 ˚C) were kept consistent across all samples. Outliers, defined as images with intensity values that were more than three scaled median absolute deviations away from the median, were removed. Images from 3-5 samples, collected over at least 3 independent experiments were analyzed for each composition. Normalized fluorescence intensity was calculated by dividing the mean fluorescence intensity by that of unlabeled SLBs.

Fluorescence Recovery after Photobleaching (FRAP)

FRAP was performed by closing the aperture to expose a small section of the field of view for 5 min, and then recording an image time-lapse of the entire area over 20-30 min. To minimize

photobleaching throughout the session, the shutter was closed between image captures. Lateral mobility of fluorescent molecules in the SLB was confirmed by observation of recovery (brightening) of the photobleached area over time (**Fig. 3.S3**).

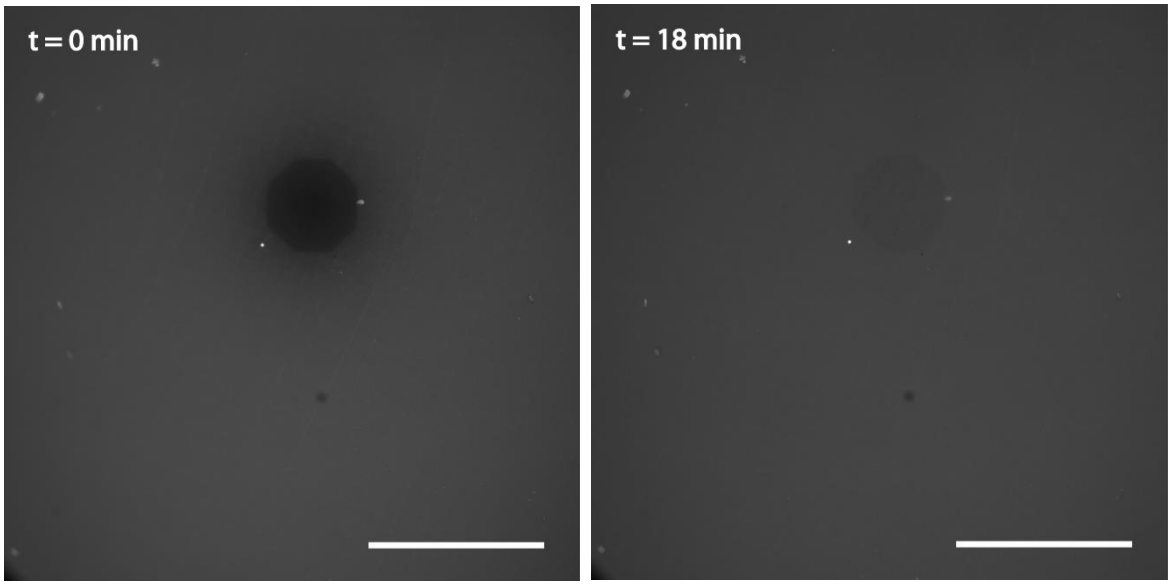

Fig. 3.S3. FRAP of a DMPC + 5 mol% DOGS-NTA (inner leaflet DMPC) SLB after incubation with MSP1D1-NLPs containing fluorescent lipid Rhodamine-B DHPE at T = 25 ˚C. More rapid recovery was observed when the temperature was raised well above the transition temperature of DMPC (Tm = 24 ˚C), to T = 33 ˚C. (scale bar = 100 μm)

Fluorescence Analysis of Vesicle Control Samples

Control SLB samples incubated with vesicles exhibited noticeable variability in the measured fluorescence intensity across the surface area of individual samples. Qualitative analysis of FM images revealed that this was due to vesicles adsorbed unevenly across the surface (**Fig. 3.S4**). No recovery was observed during FRAP, but it is possible that recovery was not detected due to the low signal to noise ratio for these samples. Nonetheless, incubation with vesicles, unlike NLPs, did not result in even incorporation of fluorescence across the SLB. Given this crucial distinction in the interaction mechanism, it was not appropriate to quantify the degree of transfer for each experimental condition as a ratio of the average fluorescent signal of SLBs incubated with NLPs compared to vesicle controls.

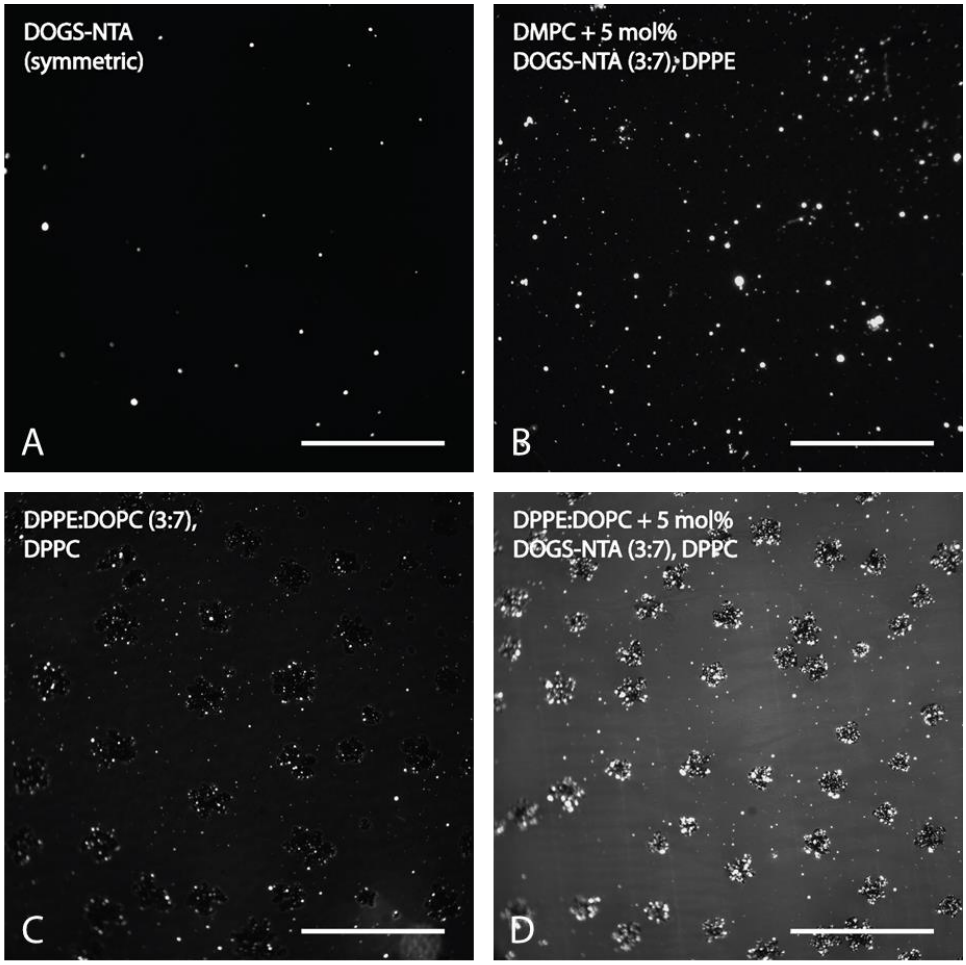

Fig. 3.S4. (A, B, C) Most FM images of SLBs after incubation with vesicles (composition: DMPC + 2 mol% Rhodamine B-DHPE) exhibited minimal fluorescence emission. (D) In limited regions, usually in close proximity to where the vesicle solution was injected, fluorescence intensity was sometimes artificially enhanced by a large number of adsorbed vesicles on the surface. Fluorescent lipids transported to SLBs from vesicles did not appear mobile (exhibited no recovery during FRAP). (scale bar = 100 µm)

References

1. El-khouri, R. J.; Bricarello, D. A.; Watkins, E. B.; Kim, C. Y.; Miller, C. E.; Patten, T. E.; Parikh, A. N.; Kuhl, T. L., pH Responsive Polymer Cushions for Probing Membrane Environment Interactions. *Nano Letters* **2011,** *11* (5), 2169-2172.
2. Zeno, W. F.; Hilt, S.; Aravagiri, K. K.; Risbud, S. H.; Voss, J. C.; Parikh, A. N.; Longo, M. L., Analysis of lipid phase behavior and protein conformational changes in nanolipoprotein particles upon entrapment in sol-gel-derived silica. *Langmuir* **2014,** *30* (32), 9780-8.
3. Blanchette, C. D.; Law, R.; Benner, W. H.; Pesavento, J. B.; Cappuccio, J. A.; Walsworth, V.; Kuhn, E. A.; Corzett, M.; Chromy, B. A.; Segelke, B. W.; Coleman, M. A.; Bench, G.; Hoeprich, P. D.; Sulchek, T. A., Quantifying size distributions of nanolipoprotein particles with single-particle analysis and molecular dynamic simulations. *J Lipid Res* **2008,** *49* (7), 1420-30.

Chapter 4: Mind the line tension – A new criteria for nanodomains in biological membranes

Amanda T. Dang[1] and Tonya L. Kuhl[2]

[1]Department of Materials Science and Engineering, University of California, Davis CA
[2]Department of Chemical Engineering, University of California, Davis CA

Publication Reference: Dang, A.T. and T.L. Kuhl, *Mind the Line Tension: New Criteria for Nanodomains in Biological Membranes.* Biophysical Journal, 2017. **112**(7): p. 1291-1292.

The compositionally diverse lipid bilayer that forms the two-dimensional fluid matrix of the cell plasma membrane is not simply a passive boundary but has functionality associated with cholesterol-related heterogeneity [94]. A key question is whether this heterogeneity leads to the coexistence of liquid-ordered (L_o) and liquid-disordered (L_d) regions on the nanometer scale [95-97]. At the moment, there is little experimental evidence of stable L_o domains (i.e. lipid rafts) in live cells [95, 98]. The work by Usery et al. establishes that there exists an abrupt transition from nanoscopic to microscopic domains in model lipid bilayers in response to minor changes in composition. Line tension was found to have a ubiquitous association with this phenomenon across a variety of lipid mixtures, presenting exciting context for why only nanoscopic heterogeneity is detected in complex biological systems.

L_o domains, which form as a result of favorable enthalpic interactions between high melting temperature lipids and sterols, are thought to occur transiently and on the order of tens of nanometers in size in biological membranes [95-96]. Early studies on detergent-resistant membranes suggested certain proteins partition preferentially into L_o compartments within the plasma membrane [95, 97], leading to pronounced interest in the properties and functional roles of lipid domains in nature. Now, 20 years past the inception of the lipid raft model [95], the underlying basis of phase separation is clear but, how this is translated in a cellular context remains obscure. The abiding mystery is sustained in large part by the inherent obstacles faced in the characterization of dynamic, nanoscopic domains in vivo [97-98]. Much

information has instead been gathered through investigation of biomimetic model systems which permit exquisite compositional control and access to a wide array of characterization techniques [96, 99-100]. The question now is how to link these mimetic, well-defined systems to cellular membranes that have a virtual zoo of different constituent molecules.

Usery et al. shed light on the correlation between lipid phase morphology and line tension by examining GUVs produced from a sweeping collection of compositionally varied quaternary phospholipid mixtures [99]. Mixtures were adjusted to contain different ratios of cholesterol, high melting point lipid, low melting point lipid known to induce nanoscopic domains, and low melting point lipid known to induce microscopic domains. A key compositional quantity, ρ, defined as the replacement ratio of the latter two components [101], was introduced as an analytical parameter for the purposes of this study. Multilamellar vesicles (MUVs) and large unilamellar vesicles (LUVs) were also employed, although size and curvature effects were found to have negligible impacts on phase behavior.

By gradually replacing low melting point lipid known to induce nanoscopic domains with low melting point lipid known to induce microscopic domains (increasing ρ value), Usery et al. showed that a stark transition from nanoscopic to micron-sized domains occurred upon reaching some critical value, ρ*. Although ρ* exhibited dependence on the types of lipids incorporated in the immediate mixture, the corresponding line tension was always ~ 0.3 pN. Through meticulous characterization, Usery et al. probed several domain properties using flicker spectroscopy [102], fluorescence measurements, small-angle neutron scattering (SANS), molecular dynamics (MD) simulations, and electron spin resonance (ESR) spectroscopy to arrive at this simple, yet cogent result. ESR spectroscopy in particular revealed that in spite of the dramatic changes observed in domain size, there was actually little variation in other characteristic properties of L_o and L_d phases (e.g. partitioning coefficient, rotational diffusion coefficient, order parameter) upon transition from nanoscopic to micron-sized domains.

In discussion, Usery et al. proposed that competing interactions arising from line tension and dipole-dipole repulsion were principle determinants of domain size. Indeed, the critical observed line tension (~ 0.3 pN) was on the order of measurements reported in separate studies on L_o-L_d phase boundaries [96, 100]. The balancing role of dipole-dipole interactions, while intuitive and also discussed in independent literature [96], was less well-defined. Another possible explanation may be that entropic fluctuations are sufficient at such low line tensions to prevent domain growth. Still, the overall body of work presented by Usery et al. should be regarded as a meaningful and detailed study on the significance of line tension in regulating the size of domains in fluid phase-separated lipid bilayers. The observation of a recurring line tension value associated with the sudden, astonishing increase in domain size across multiple lipid mixtures inspires an intriguing framework for continued research beyond biomimetic model systems. In environments as complex as native plasma membranes, do line tension-dominated mechanisms of phase separation lead to the widespread formation of compositionally distinct, but similarly sized L_o nanodomains? Is the critical line tension altered by the presence of proteins which partition preferentially into L_o phases [103]? If so, could biology make use of modulations in line tension to coordinate cell processes? There is ample opportunity to build upon this extensive and compelling work by Usery et al.

We thank Dr. Anne Kenworthy and Dr. Krishnan Raghunathan for generously sharing their insight on this subject.

References

1. Lingwood, D. and K. Simons, *Lipid rafts as a membrane-organizing principle.* Science, 2010. **327**(5961): p. 46-50.
2. Levental, I. and S.L. Veatch, *The Continuing Mystery of Lipid Rafts.* Journal of Molecular Biology, 2016. **428**(24, Part A): p. 4749-4764.
3. Sriram, I. and D.K. Schwartz, *Line tension between coexisting phases in monolayers and bilayers of amphiphilic molecules.* Surface Science Reports, 2012. **67**(6): p. 143-159.
4. Day, C.A. and A.K. Kenworthy, *Tracking microdomain dynamics in cell membranes.* Biochimica et Biophysica Acta (BBA) - Biomembranes, 2009. **1788**(1): p. 245-253.
5. Swamy, M.J., et al., *Coexisting domains in the plasma membranes of live cells characterized by spin-label ESR spectroscopy.* Biophysical Journal, 2006. **90**(12): p. 4452-4465.
6. Usery, R.D., et al., *Line tension controls liquid-disordered + liquid-ordered domain size transition in bilayers.* Biophysical Journal, 2017.
7. Honerkamp-Smith, A.R., et al., *Line Tensions, Correlation Lengths, and Critical Exponents in Lipid Membranes Near Critical Points.* Biophysical Journal, 2008. **95**(1): p. 236-246.
8. Konyakhina, T.M., et al., *Control of a Nanoscopic-to-Macroscopic Transition: Modulated Phases in Four-Component DSPC/DOPC/POPC/Chol Giant Unilamellar Vesicles.* Biophysical Journal, 2011. **101**(2): p. L8-L10.
9. Esposito, C., et al., *Flicker Spectroscopy of Thermal Lipid Bilayer Domain Boundary Fluctuations.* Biophysical Journal, 2007. **93**(9): p. 3169-3181.
10. Lorent, J.H. and I. Levental, *Structural determinants of protein partitioning into ordered membrane domains and lipid rafts.* Chemistry and Physics of Lipids, 2015. **192**: p. 23-32.

Chapter 5: Theoretical Interaction Energies between a Silica Surface and a Phospholipid Bilayer

Project Background

In a collaboration with Dr. Daryl Y. Sasaki's group (Sandia National Laboratory), we investigated the phenomenon of acid-triggered hole and blister formation in silica-supported SLBs.[1] The following is a reformatted excerpt from my contribution to the project, which describes the theoretical van der Waals, electrostatic, and combined interaction energies per unit area between a silica surface and a phospholipid bilayer as a function of separation distance (*d*), modeled as two flat surfaces interacting across an aqueous medium of known dielectric constant (ϵ_r=78).

Electrostatic Energy Contribution

The electrostatic energy contribution was calculated as the numerical solution to the Poisson-Boltzmann equation for two flat surfaces (Equation 1):

$$\nabla^2\Psi = \sigma/(\epsilon_r\epsilon_0) \quad \text{(Equation 1)}$$

Where Ψ is the electrostatic potential, σ is the surface charge density, ϵ_r is the dielectric constant of the aqueous solution, and ϵ_0 is the vacuum permittivity. To estimate the surface potential and surface charge density values for RCA-cleaned glass at infinite separation, I measured the zeta potential of colloidal analogues for each material (see below). Using RCA-cleaned silica beads, I observed a negative zeta potential at the silica-water interface that was consistent with values reported in the literature[2]. Using vesicles comprised of POPC and cholesterol, I detected a minor negative charge, even in the absence of negatively charged fluorescent lipid TR-DHPE. Although PC lipids are zwitterionic, previous work has shown that many pure lipid mixtures typically register a small negative zeta potential[3].

I present the theoretical calculations for a negatively charged membrane and an electroneutral membrane using two sets of boundary conditions. In **Fig. 5.1A** and Fig. **5.1B**, assuming a fixed surface potential results in a net attractive electrostatic interaction. Conversely in **Fig. 5.1C** and Fig. **5.1D**, assuming a fixed surface charge density results in a minor repulsive interaction.

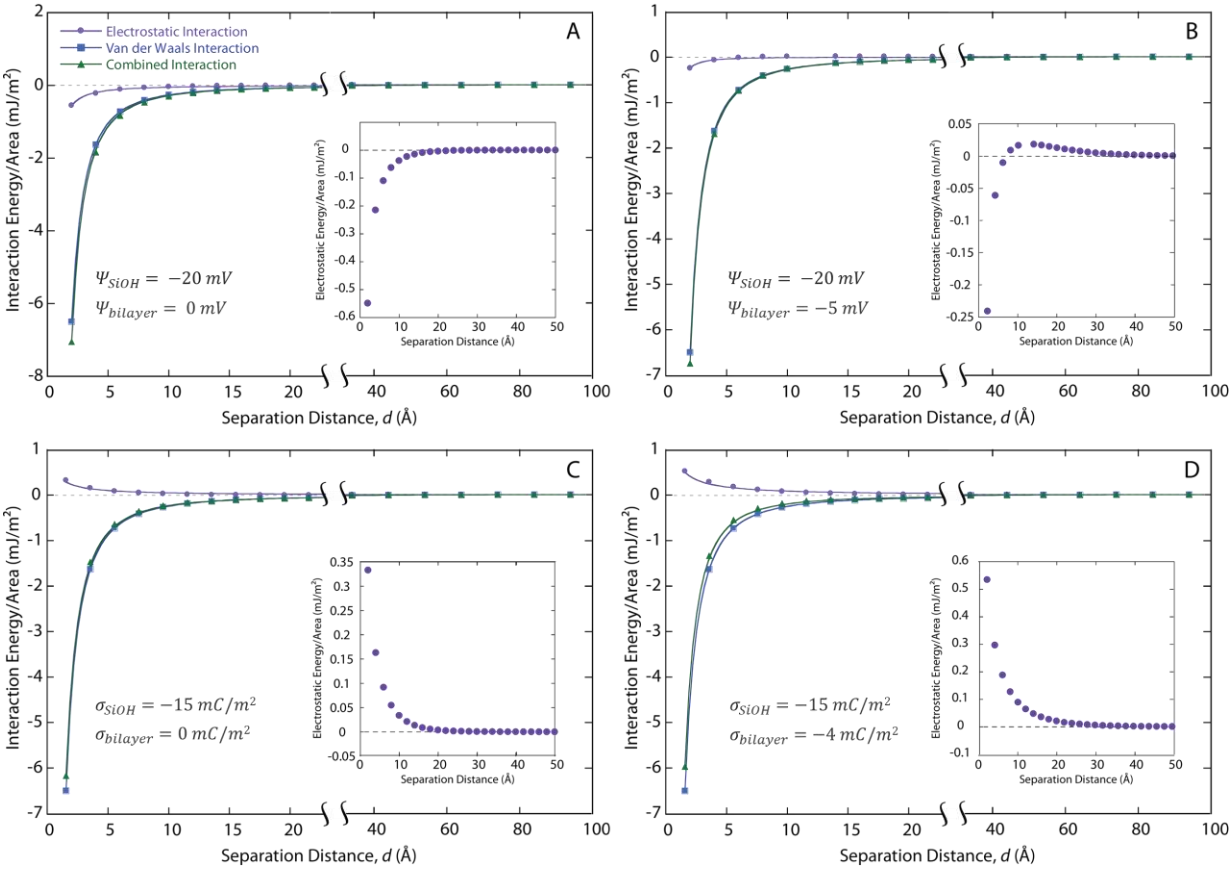

Fig. 5.1. The theoretical electrostatic (purple circles), van der Waals (blue squares), and combined interaction energies (green triangles) between a negatively charged silica surface (Ψ_{silica}= -20 mV; σ_{silica}= -15 mC/m^2) and a supported lipid bilayer as a function of average separation distance, *d*, in a solvent containing a monovalent salt concentration of 110 mM (Debye length ~0.9 nm). Electrostatic contributions (magnified in insets) were calculated as the numerical solution to the Poisson-Boltzmann equation assuming (A) fixed surface electrostatic potential boundary conditions and an electroneutral membrane, (B) fixed surface electrostatic potential boundary conditions and a negatively charged membrane, (C) fixed surface charge density boundary conditions and an electroneutral membrane, (D) fixed surface charge density boundary conditions and a negatively charged membrane.

Van der Waals Energy Contribution

In all cases, short-ranged van der Waals interactions ultimately dominate due to the screening of electrostatic interactions in high salt concentration conditions (Debye length ~9 Å). The van der Waals contribution was calculated analytically using the classical expression for the interaction energy per unit area for two flat surfaces (Equation 2)[4]:

$$W_{vdW} = (-A)/(12d^2) \qquad \text{(Equation 2)}$$

Where W_{vdW} is the van der Waals interaction energy per unit area, d is the separation distance, and A is the Hamaker constant. The Hamaker constant was estimated using experimental refractive index values attained by Kienle et al[5]. The combined interaction was determined as the linear combination of the electrostatic and van der Waals energy contributions.

Zeta Potential Measurement

Zeta potential measurements for RCA-cleaned silica beads and lipid vesicles were recorded using a Malvern Zetasizer (**Table 5.1**). For each sample, the zeta potential was measured with the solvent (citrate-phosphate buffer) adjusted to pH 7.4, and then again upon adjustment to pH 5. Dynamic light scattering (DLS) was used to determine the average particle size and distribution of the vesicle samples.

Table 5.1. Zeta Potential Measurements

Sample	Average Particle Size [nm]	Zeta Potential, pH 7.4 [mV]	Zeta Potential, pH 5 [mV]
POPC:Chol (7:3) + 0.3 mol% TR-DHPE	254 ± 20.7	-2.74 ± 0.838	-3.14 ± 1.08
POPC:Chol (7:3)	266 ± 52.2	-1.80 ± .519	-1.98 ± 0.930
RCA-cleaned silica beads (Polysciences, Inc.)	400 ± 40 *	- 21.7 ± 1.16	- 23.03 ± 1.08

* Manufacturer specifications

Determining Surface Charge Density from Zeta Potential

The corresponding surface charge density for a given surface potential value, estimated using the measured zeta potential, was determined by examining the numerical solution to the Poisson-Boltzmann equation at infinite separation (**Fig. 5.2**):

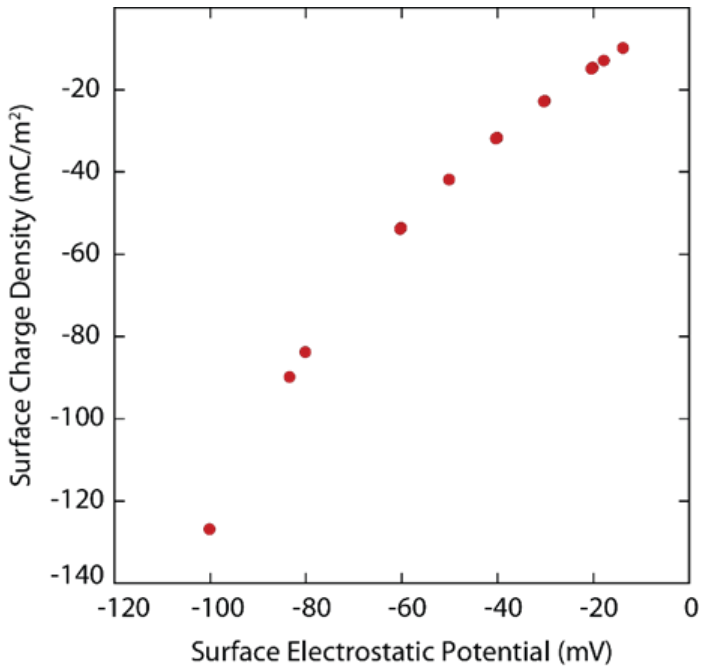

Fig. 5.2: Theoretical surface charge density corresponding to a given surface potential value, calculated as the numerical solution to the Poisson-Boltzmann equation for two surfaces at infinite separation.

References

1. Dolstra, C. C., et al. (2019). "Mechanism of Acid-Triggered Cargo Release from Lipid Bilayer-Coated Mesoporous Silica Particles." Langmuir.
2. Alves-Junior, J.A. and J.B. Baldo, *The Behavior of Zeta Potential of Silica Suspensions.* New Journal of Glass and Ceramics, 2014. **04**(2): p. 9.
3. Kurniawan, J., et al., *Interaction Forces between Ternary Lipid Bilayers Containing Cholesterol.* Langmuir, 2014. **30**(17): p. 4997-5004.
4. Israelachvili, J., *Intermolecular and Surface Forces*. 3 ed. 1991: Academic Press.
5. Kienle, D.F., et al., *Thickness and refractive index of DPPC and DPPE monolayers by multiple-beam interferometry.* Anal Bioanal Chem, 2014. **406**(19): p. 4725-33.

Chapter 6: Experimental Considerations

The following is a compilation of miscellaneous experimental notes intended to inform future studies related the body of work presented in this dissertation.

Fabrication of PAA-cushioned Supported Lipid Bilayers

- Extensive notes on preparation and characterization of SLBs can be found in a tutorial by Kurniawan et al.[1], for which I provided fluorescence microscopy and atomic force microscopy data and analysis.
- LB/LB was ideal for formation of high quality SLBs directly on hard substrates (e.g. glass, mica), but resulted in delamination when used to deposit bilayers on PAA cushions. Successful deposition onto PAA cushions required LB/LS.
- PAA cushions were reusable and could be cleaned with Hellmanex and ethanol.
- Due to the polar headgroup, DPPE lipid solutions were typically dissolved in mixtures of $CHCl_3$ and MeOH, whereas other lipid mixtures were dissolved in pure $CHCl_3$. DPPE solutions were also typically given extra time to warm up to room temperature to ensure full solubilization before spreading.
- APTES solutions were not used if precipitates were visible in the bottle or if the solution was turbid. Fresh solutions were used whenever possible.
- All PAA cushion fabrication steps, with the exception of curing, where performed in the laminar flow cabinet to prevent contamination.

AFM of Supported Lipid Bilayers and Nanolipoprotein Particles

- Tapping mode AFM was used to image all surfaces. Contact mode was only used to determine the location of the surface along the (normal) z-axis, and to verify the presence of a bilayer by mechanically removing a small patch of membrane and checking for a ~5 nm step height.

- AC240 silicon nitride tips were compatible with SLB surfaces. However, addition of NLPs or vesicles would result signal disruption due to adsorption or particles to the cantilever.
- To mount mica-supported SLBs in the Asylum liquid sample holder (designed for 0.5" diameter circular glass coverslips), mica freshly cleaved and glued onto a circular coverslip using epoxy resin. Previous attempts to use vacuum grease and double-sided tape tended to resulted in contamination of the buffer or delamination.

Fluorescence Microscopy of SLBs

- Confocal fluorescence microscopy and total internal reflection fluorescence (TIRF) microscopy were tested as alternative imaging methods for fluorescently labeled SLBs and SLBs incubated with fluorescently labeled NLPs. However, the signal strength from the membrane was too low to achieve an appreciable signal using the available instrument (Olympus FV1000 Laser Scanning Confocal).
- Background fluorescence from silica-based substrates should be measured and subtracted accordingly when quantifying the average fluorescent intensity of SLBs. The signal-to-noise ratio was especially low when using silica-based substrates and a FITC filter cube (dichroic cut-on λ=506 nm), so SLBs labeled with corresponding dyes (e.g. Oregon Green™) were typically patterned to present well-defined geometric features for identification. Background noise was also reduced by imaging in a dark room and by storing samples in container made of black Delrin® during imaging.

UV-Ozone Patterning of Supported Lipid Bilayers

- SLBs were patterned by exposing surfaces to UV emission through a photomask. Throughout the patterning process (~30 min), the SLBs and photomask were kept submerged in DI water contained in a quartz dish. The UV source was typically mounted (outside of the quartz dish) directly underneath the sample to maximize the intensity of exposure.

- Attempts to achieve the same effect using a UV-ozone chamber were unsuccessful, possibly because the light source was fixed too far from the surface or because ozone accumulation in the chamber resulted in degradation of the sample.
- PAA-cushioned SLBs could be patterned before or after bilayer deposition. If patterned before forming the membrane (dry cushion only), UV-ozone patterning could be performed in air. Note that this option would often result in sample heating due to the long exposure time.
- Pre-patterning the PAA before bilayer deposition often resulted in instances where the bilayer "sealed" the PAA patches from the bulk solution.
- Exposed regions could be readily passivated against non-specific protein and lipid adsorption using BSA or a siliconizing fluid (e.g. Aquasil). SLBs deposited onto passivated, patterned, PAA-cushioned surfaces sometimes formed continuous bilayers by "bridging" across the passivated regions.
- SLBs should be kept in lipid-saturated conditions for long-term storage to prevent solubilization of lipid into the buffer/subphase over time.

Fabrication and Characterization of Nanolipoprotein Particles

- Cell-free expression was most successful when the total reaction volume was between 500 – 1000 µL. Protein yield was observed to decrease when we scaled down to conserve materials.
- MP-NLPs formed with polymeric stabilizers (e.g. telodendrimers) sticking out from the disc bilayer were not observed to interact with SLBs when characterized using AFM. The result suggested that membrane-to-membrane contact was important for lipid/protein transfer from NLPs to SLBs, but was not explored conclusively in this work.
- NLPs should not be stored in deionized water. Unpublished DLS results showed that high ionic (~100 mM) strength was necessary to prevent particle aggregation. NLPs were stable in Tris and PBS buffer.

- NLPs appeared to aggregate slowly over time when stored in buffer, even with sufficiently high ionic strength. Samples aged over a week are not recommended for use, although vortexing and quick sonication can be used to re-disperse samples if fresh NLPs are not available.
- DLS and UV-Vis spectroscopy measurements were typically convoluted by signal contributions from vesicles, likely originating from a small population of NLPs that were in a dissociated state (comprised of free lipids and partially water-soluble apolipoprotein). While it was possible to gather an approximate concentration based on a de-convoluted spectrum and SDS-PAGE results, specific quantification assays (e.g. ELISA) and size exclusion chromatography were most accurate and ideal. When more accurate options were unavailable, batch-based experiments were selected to ensure that NLP concentration was consistent across all trials.
- Apolipoproteins can be labeled with BODIPY fluorescent dye during cell-free expression using FluoroTect^{TM} Green$_{Lys}$ *in vitro* Translation Labeling System (Promega). While this dye was effective at enabling "in-gel" detection during SDS-page, it was too weak to produce a clear signal during wide-field fluorescence microscopy, confocal fluorescence microscopy, and TIRF microscopy of NLPs bound to a SLB surface (via DOGS-NTA linker groups).
- NLPs should be stored at 4 °C when not in use. "Empty" NLPs without embedded MPs are durable enough for storage under freezing conditions (-20 °C), but should be checked for stability if subjected to several freeze-thaw cycles. Empty NLPs are also amenable to lyophilization (no attempts were made to lyophilize MP-NLPs). Once lyophilized, NLPs can be placed in -20 °C for long-term storage.

Incubation of SLBs with NLPs

- Samples were constrained to small volumes by either using custom-machined holders or by incubating in an "inverted drop" formed between the sample (oriented upside down) and an underlying surface.

- *In situ* cell-free expression of NLPs in the presence of a SLB resulted in degradation of the SLB, likely due to exposure to enzymes or other lipid-soluble components in the cell lysate mixture.
- During long incubation periods, samples were stored in a sealed container with a wet paper towel to prevent evaporation.

1. Kurniawan, J.; Ventrici de Souza, J. F.; Dang, A. T.; Liu, G.-y.; Kuhl, T. L., Preparation and Characterization of Solid-Supported Lipid Bilayers Formed by Langmuir–Blodgett Deposition: A Tutorial. *Langmuir* **2018,** *34* (51), 15622-15639.